TRYPTOPHAN METABOLITES ARE ASSOCIATED WITH GUT-BRAIN ALTERATIONS IN FUNCTIONAL DYSPEPSIA

AUTHORS

Matthias Ceulemans[1,2], Lucas Wauters[1,3], Nathalie Weltens[1,4], Greet Vandermeulen[1], Henriette de Loor[5], Pieter Evenepoel[5,6], Raul Y Tito[7,8], Arnau Vich Vila[7,8], Muriel Derrien[7,8], Boushra Dalile[9], Jan Tack[1,3], Kristin Verbeke[1], Jeroen Raes[7,8,#], Lukas Van Oudenhove[1,4,#], Tim Vanuytsel[1,3,#,*]

AFFILIATIONS

1) Translational Research Center for Gastrointestinal Disorders (TARGID), Department of Chronic Diseases and Metabolism (ChroMeta), KU Leuven, Leuven, Belgium

2) Precision Immunology Institute, Icahn School of Medicine at Mount Sinai, New York, NY

3) Gastroenterology and Hepatology, University Hospitals Leuven, Leuven, Belgium

4) Laboratory for Brain-Gut-Axis Studies (LaBGAS), KU Leuven, Leuven, Belgium

5) Nephrology and Renal Transplantation Research Group, Department of Microbiology, Immunology and Transplantation, KU Leuven, Leuven, Belgium

6) Nephrology and Renal Transplantation, University Hospitals Leuven, Leuven, Belgium

7) Laboratory of Molecular Bacteriology, Department of Microbiology, Immunology and Transplantation, Rega Institute, KU Leuven, Leuven, Belgium.

8) Center for Microbiology, Vlaams Instituut voor Biotechnologie (VIB), Leuven, Belgium.

9) Laboratory of Biological Psychology, KU Leuven, Belgium

# Senior authors contributed equally

* Correspondence to: Tim Vanuytsel, MD, PhD, University Hospitals Leuven, Herestraat 49, 3000 Leuven, Belgium. e-mail: tim.vanuytsel@uzleuven.be

Abstract

Background and aims

Microbiota is thought to contribute to the pathophysiology of disorders of gut-brain interaction, including functional dyspepsia (FD), although comprehensive human data covering the entire microbiota-gut-brain axis are scarce. We aimed to study the relationships among microbiota-produced metabolites including tryptophan metabolites and short-chain fatty acids (SCFA), and functional brain connectivity in FD, in relation to symptomatology.

Methods

In 46 patients with Rome IV-diagnosed FD and 30 healthy controls (HC), targeted metabolomics using chromatography and mass spectrometry was conducted to quantify metabolites in blood, urine, and stool. Associations with gut microbiota and symptomatology were tested using 16S rRNA gene sequencing-based fecal quantitative microbiota profiling and validated symptom questionnaires. Resting-state functional magnetic resonance imaging in 27 patients and 36 HC enabled analysis of functional connectivity in selected brain networks.

Results

Patients with FD exhibited distinct profiles of tryptophan metabolites and SCFA with higher urinary indole-3-acetate (IAA, P=0.018), lower serum kynurenine (P=0.030) and lower plasma propionate (P=0.0055) concentrations. FD-specific metabolite alterations were associated with more severe GI and psychological symptoms. The fecal microbiota profile was similar between FD and HC. Complementary analyses demonstrated significant alterations in resting-state brain connectivity of 44 predefined regions between FD and HC, while a connectivity-based classifier could accurately discriminate FD from HC (96% sensitivity, 100% specificity). Differences in connectivity measures mediated the higher urinary IAA levels in FD.

Conclusion

Dysregulated functional brain connectivity in FD supports an objective diagnosis, while alterations in specific tryptophan metabolite and SCFA levels highlight their potential as prognostic, predictive, or therapeutic biomarkers, and warrant further investigation on microbiota modulating therapies for FD.

ClinicalTrials.gov identifier: NCT03545243

Introduction

Functional dyspepsia (FD) is a chronic condition characterized by specific meal-related and painful symptoms perceived in the gastroduodenal region. Diagnosed by the Rome IV criteria in the absence of any organic or structural disease, hallmark FD symptoms include postprandial fulness, early satiation, epigastric pain and burning[1]. With an estimated worldwide prevalence of over 7%, FD affects considerably more individuals than irritable bowel syndrome (IBS)[2], despite more limited public awareness in comparison. Both functional gastrointestinal (GI) disorders were recently relabeled as disorders of gut-brain interaction (DGBI)[3], to better reflect their pathophysiology, presumed to involve dysfunction of intricate gut-brain interplay. Besides an impaired quality of life[4] and common overlap with psychological distress[5], FD imposes a substantial socio-economic burden due to repeated healthcare visits and a lack of cost-effective treatment options[6], highlighting the pressing need for increased insight in its pathophysiology to support clinical diagnosis and guide therapy selection.

Research on pathophysiological mechanisms underlying FD symptoms has primarily focused on mucosal immune activation[7], epithelial barrier defects[8] and gut microbial alterations[9]. Specific microbial shifts were found in the proximal GI tract[10], with most evidence for duodenal microbial changes, including increased abundance of *Streptococcus*[10] and reduced *Firmicutes*[11], *Neisseria*[12] and *Porphyromonas*[12] abundance in FD compared to controls. In addition, an independent association between the onset of FD and psychosocial factors such as anxiety and mood disorders suggests an important role of gut-brain communication[13]. This gut-brain crosstalk can potentially be influenced by the gut microbiota through diverse mechanisms. Among these, the main metabolites produced by gut microbes, most notably short-chain fatty acids (SCFA) and aromatic amino acid (AAA; tryptophan, phenylalanine and tyrosine) metabolites, are thought to directly or indirectly play a role in various homeostatic processes including gut-microbiota communication[14, 15]. However, human data on the role of microbial metabolites in altered microbiota-gut-brain crosstalk in FD are currently lacking.

To investigate the contribution of specific microbial metabolites to gut-brain interactions in FD, we performed targeted metabolomic and fecal microbiota profiling in a prospectively recruited cohort of patients with FD and matched healthy controls (HC). Furthermore, we combined extensive symptom profiling and functional magnetic resonance imaging (fMRI) of the brain to evaluate central alterations related to FD pathophysiology. Lastly, using regression, classification and mediation models, we identified a link between microbiota-derived metabolites, symptom profiles, and functional brain alterations.

Methods

Study design and participants

Patients with Rome IV-defined FD (n=46) and matched healthy controls (HC) (n=30) were prospectively recruited in a single center to undergo sampling of blood, urine and feces for extensive metabolite and microbiota profiling. In- and exclusion criteria are listed in the **Supplementary Methods**. During the study visit, participants underwent extensive profiling of GI and extraintestinal symptoms (**Supplementary Methods**). Macronutrient intake was estimated through a validated online food frequency questionnaire (FFQ), reporting average daily total energy (kCal/day), protein (g/day), carbohydrate (g/day), fiber (g/day), fat (g/day) and water (mL/day) intake[16]. The study was approved by the University Hospitals / KU Leuven Ethics Committee for Research (S60953, S60984) and registered at ClinicalTrials.gov (NCT03545243). All participants provided written informed consent before the start of the study. The study was conducted in accordance with the Declaration of Helsinki and the Guidelines for Good Clinical Practice.

Sample collection

During study visits, qualified staff collected blood samples in fasted state (≥ 6h) in EDTA and SST tubes (both BD Vacutainer) for plasma and serum collection, respectively. Blood samples were centrifuged, aliquoted, and plasma and serum were stored at -80°C until further processing. Participants provided a fasted spot urine sample, which was stored at -80°C until analysis. Within two days of the study visit, participants collected a stool sample at home in a container provided for this purpose, which was immediately frozen (-18°C) at participants' own freezer and transported to the lab with ice packs, where samples were stored at -80°C until analysis. Participants scored the consistency of their stool sample using the Bristol Stool Scale (BSS) as a proxy for intestinal transit time[17]. A subset of participants underwent resting state functional magnetic resonance imaging (rs-fMRI) as part of the study.

Targeted metabolite analyses

A selected panel of aromatic amino acids (AAA), host and microbial AAA metabolites, and uremic toxins (**Figure 2A**) was quantified via ultra-performance liquid chromatography-tandem mass spectrometry as previously published[18] on spot urine samples and fasted serum samples. Creatinine was measured in urine samples via routine enzymatic assay, and urinary metabolite concentrations were normalized to creatinine levels to mitigate dilution effects. Measurement of short-chain fatty acids (SCFA) was performed as previously described

following optimized gas chromatography-mass spectrometry protocols for frozen fecal[19] and fasted plasma samples[20].

Fecal microbiota analysis

Quantitative microbial profiles (QMP) were obtained by combining 16S rRNA V4 gene sequencing and microbial load quantification as described before[21, 22] (**Supplementary Methods**). This allowed for the investigation of absolute fecal microbial differences between groups, as well as associations between the gut microbiota and psychological and metabolic metadata.

Functional magnetic resonance imaging

Optional rs-fMRI measurements were performed in consenting individuals (27 patients with FD and 20 HC) at the University Hospitals Leuven Radiology Department using a 3T Philips Achieva DStream MRI scanner (32-channer head coil). The dataset was complemented with rs-fMRI measurements of a previously recruited cohort of 16 additional HC who underwent identical fMRI procedures. Processing and analysis of fMRI data are described in the **Supplementary Methods**.

Statistical analyses

Statistical analyses were performed in R (v4.5.1). Additional details are provided in the **Supplementary Methods**. Patient characteristics were compared between groups (FD vs. HC) by unpaired Wilcoxon tests for continuous data and Fisher's exact tests for categorical data. Linear regression models were used to analyze between-group differences of metabolite, microbiota, dietary or symptom data. Relative levels (z-scored) of individual SCFA were summed to analyze total SCFA levels in parallel with individual SCFA levels. Similarly, AAA and their metabolites were z-scored and aggregated per origin (**Figure 2A**). Effect sizes were calculated per independent variable and reported as partial eta squared values (η_p^2). For targeted analyses (dietary, symptom and metabolite data), nominal P values were calculated for each main effect and included in figures, with $P < 0.05$ considered statistically significant and $P < 0.1$ considered a trend. Targeted analyses with persisting significance after multiple testing correction (false discovery rate-adjusted q-values, q_{FDR}) are indicated separately. Principal component analysis (PCA) based on Euclidean distance and permutational analysis of variance (PERMANOVA) was performed on scaled (z-scored) individual metabolite data measured in serum or in urine to evaluate global between-group differences in metabolite profiles.

Alpha diversity indices (within-sample; observed richness, Shannon index, inverse Simpson index) were analyzed at the genus-level QMP matrix. Beta (between-sample) diversity was analyzed by principal coordinate analysis (PCoA) based on Bray-Curtis dissimilarity at the genus level. Differential absolute genera abundance analysis was performed on the genus-level QMP matrix after excluding unclassified taxa at the genus level and applying a prevalence cutoff of ≥ 20% across all samples. Exploratory analysis with Mann-Whitney-U tests and Benjamini-Hochberg correction preceded detailed analyses using negative binomial models. First, univariable model was constructed to analyze between-group differences, followed by multivariable models including 'group' (FD vs. HC), 'PPI intake' and 'BSS category'. Benjamini-Hochberg correction was applied per dependent variable to adjust for multiple simultaneous comparisons and presented as nominal p-values (*P*) and false discovery rate-adjusted *q*-values (q_{FDR}). Parameter estimates and standard error (B ± SE) are reported.

Correlation analyses were performed by calculation of Spearman's correlation coefficient. Correlations with microbial taxa were performed including taxa with a prevalence of ≥ 20% across the samples (68 taxa) unless specified otherwise. Benjamini-Hochberg correction was applied for the number of tests equaling the number of Y-variables (symptoms or fecal genera) included.

Results

High psychological symptom burden in FD

To investigate the contribution of gut microbial metabolites to the pathophysiology of FD, we studied a well-characterized cohort of 46 patients with Rome IV-diagnosed FD and 30 HC. The absence of endoscopic alterations was confirmed during esophagogastroduodenoscopy in all participants. The characteristics of this cohort have been described before[23] (**Supplementary Table 1**). Briefly, patients and controls were matched for age, sex, body mass index (BMI), and geographic origin (all $P > 0.1$). Thirty nine percent of patients with FD (n = 18/46) were taking PPI at the time of sampling, while none of the HC were taking PPI. As reported before[12], food frequency questionnaires revealed differences in dietary patterns between study groups, with lower estimated intake of fiber ($\eta_p^2 = 0.12$, $P = 0.015$, $q_{FDR} = 0.045$) and protein ($\eta_p^2 = 0.21$, $P = 0.0012$, $q_{FDR} = 0.0071$) in FD compared to HC. Intake of other macronutrients and total energy intake was similar in FD (all $P > 0.1$) (**Supplementary Table 2**).

First, we confirmed the previously described psychological symptom burden of FD[5] in this cohort, evidenced by significantly higher symptom scores for anxiety (GAD7; $\eta_p^2 = 0.35$, $P < 0.0001$), perceived stress (PSS; $\eta_p^2 = 0.21$, $P = 0.0004$), depression (PHQ9; $\eta_p^2 = 0.69$, $P < 0.0001$), extraintestinal symptoms (PHQ12; $\eta_p^2 = 0.59$, $P < 0.0001$), GI-specific anxiety (VSI; $\eta_p^2 = 0.70$, $P < 0.0001$) and posttraumatic stress (PTSD; $\eta_p^2 = 0.28$, $P < 0.0001$) in patients with FD in comparison to HC, besides more severe GI-specific symptoms (LPDS; $\eta_p^2 = 0.67$, $P < 0.0001$ and PAGI-SYM; $\eta_p^2 = 0.73$, $P < 0.0001$) as anticipated **(Figure 1**). Patients with FD also presented with lower positive affect (PANAS+; $\eta_p^2 = 0.22$, $P = 0.0002$) and higher negative affect (PANAS-; $\eta_p^2 = 0.22$, $P = 0.0001$) scores **(Figure 1**). All differences in symptom scores persisted after multiple testing correction (all $q_{FDR} < 0.0005$). Childhood trauma severity (CTQ) was not elevated in FD ($\eta_p^2 = 0.006$, $P = 0.51$). PPI intake was not associated with alterations in any of the GI or extraintestinal symptom measures (all $P > 0.1$), reflecting that patients with FD taking PPI were symptomatic, as per inclusion criteria for this study (**Supplementary Table 3**).

Patients with FD exhibit a distinct metabolite profile

We measured the concentrations of a relevant selection of host and microbiota-derived aromatic amino acids (AAA) and key AAA metabolites (**Figure 2A**) using targeted ultra-performance liquid chromatography-tandem mass spectrometry. First, we looked at the overall serum metabolite composition. Principal component analysis (PCA) and permutational analysis of variance (PERMANOVA) revealed a significantly distinct serum-derived metabolic signature between FD and HC ($R^2 = 0.031$, $P_{PERMANOVA} = 0.012$) (**Figure 2B**). When only including microbial AAA metabolites, the serum metabolite signature was again different

between FD and HC (R^2 = 0.033, $P_{PERMANOVA}$ = 0.030) (**Supplementary Figure 1A**). The urinary AAA metabolite profile was not different between both groups (R^2 = 0.024, $P_{PERMANOVA}$ = 0.11) (**Supplementary Figure 1B**). However, similarly to the serum results, the profile of microbial AAA metabolites in urine differed significantly between FD and HC (R^2 = 0.037, $P_{PERMANOVA}$ = 0.040) (**Figure 2C**).

Next, the concentrations of analyzed molecules were standardized and aggregated by their origin, i.e. AAA, host-derived AAA metabolites and microbial AAA metabolites (**Figure 2A**), to assess differences in metabolites based on their origin. To mitigate the potential confounding effects of dietary or PPI intake, all models were adjusted for protein intake and PPI use. Serum (η_p^2 = 0.10, P = 0.027) but not urinary host AAA metabolites (η_p^2 = 0.00004, P = 0.97) were lower in FD (**Figure 2D-E**). In line with PCA results presented before, urinary microbial AAA metabolite levels (η_p^2 = 0.11, P = 0.033) were higher in FD (**Figure 2E**). Interestingly, protein intake was associated with serum microbial AAA metabolite levels (η_p^2 = 0.12, P = 0.017) but not with urinary levels, nor with host AAA metabolite levels in serum or urine. Systemic and urinary AAA levels were similar between groups (all P > 0.1) (**Figure 2D-E**). On the individual metabolite level, lower serum kynurenine (Kyn) (η_p^2 = 0.10, P = 0.030) concentrations were measured in FD while serum phenylalanine (η_p^2 = 0.09, P = 0.038), serum and urinary phenylacetylglutamine (PAGln) (η_p^2 = 0.09, P = 0.043; η_p^2 = 0.12, P = 0.030), and urinary indole-3-acetate (IAA) (η_p^2 = 0.14, P = 0.018) levels were higher in FD (**Figure 2F**). Only the differences in metabolite groups (serum host-derived metabolites: q_{FDR} = 0.081, urinary microbial metabolites: q_{FDR} = 0.098) tended to persist after multiple testing correction.

SCFA are key metabolites produced by the gut microbiota from carbohydrate fermentation. Fecal and plasma main SCFA (acetate, butyrate, propionate) were analyzed using gas chromatography-mass spectrometry. Concentrations of all measured individual and total SCFA in both feces and plasma were on average lower in FD compared to HC (**Figure 2G-H**). Lower systemic levels of propionate (η_p^2 = 0.16, P = 0.0055, q_{FDR} = 0.011) and total SCFA (η_p^2 = 0.17, P = 0.0044, q_{FDR} = 0.011) reached statistical significance, independent of PPI and fiber intake, the major substrate for SCFA production (**Figure 2H**).

IAA, propionate and Kyn are associated with gastrointestinal and comorbid psychological symptoms in FD

Gut microbial-derived IAA was recently shown to relay psychological stress to the gut in mice, while increased IAA levels in patients with major depressive disorder demonstrated its relevance in a human context[24]. Therefore, we subsequently interrogated whether the distinct metabolic profile in patients with FD, specifically increased microbial AAA metabolite levels

including IAA, as well as decreased propionate, was associated with the GI-specific and extraintestinal symptom profile in our cohort.

To explore the clinical relevance of altered metabolites, we performed correlation analyses between symptom outcomes and all measured metabolites in this cohort. Consistently, urinary IAA, plasma propionate and serum Kyn were among the metabolites most strongly associated with symptomatology (**Figure 3A**, **Supplementary Table 4**). Hence, we constructed linear regression models and added dietary protein (IAA, Kyn) or fiber (propionate) and PPI intake as covariates to assess associations between IAA, propionate and Kyn, with participants' GI and comorbid psychological symptoms. Urinary IAA was significantly associated with general anxiety, depression, extraintestinal and GI-specific (LPDS) symptoms in a univariable model (**Figure 3B**, **Supplementary Table 5**), confirming the previously suggested link between IAA and psychological distress[24]. Similar trends were found for anxiety, depression, perceived and post-traumatic stress, extraintestinal and GI-specific (LPDS, PAGI-SYM) symptoms in the corrected model, although they did not survive multiple testing correction, indicating that associations were largely independent of protein intake and PPI use. Plasma propionate levels were significantly and inversely associated with symptom levels except for perceived stress, with significance persisting in multivariate analyses accounting for fiber and PPI intake (**Figure 3C**, **Supplementary Table 5**). Similarly, serum Kyn, a tryptophan metabolite of non-microbial origin, was inversely associated with symptoms except for GI-specific anxiety (**Figure 3D**, **Supplementary Table 5**). Multivariable models including protein and PPI intake further increased the significance of all symptom associations, while protein intake was highly associated with Kyn concentrations as well. Hence, Kyn levels were associated with GI and extraintestinal symptoms independent of dietary protein, although additional variation was explained by protein intake.

Of note, urinary IAA, plasma propionate and serum Kyn were only minimally correlated with each other, suggesting their associations with symptoms might be independent (**Figure 3E**). To assess the individual contribution of each metabolite of interest on the different symptom variables, we used multiple linear regression analysis with correction for fiber and protein intake. While urinary IAA was strongly associated with depression, extraintestinal and general GI symptoms, the association between plasma propionate with upper-GI symptoms, general and GI-specific anxiety, and both positive and negative affect had the highest effect sizes, with minimal additional contribution of serum Kyn to each of the symptom variables (**Figure 3F**, **Supplementary Table 6**).

The fecal microbiota in FD is similar compared to HC and shaped by intestinal transit time

We next interrogated whether the shifts in specific metabolites were linked to alterations in the gut microbiota. To this end, we performed quantitative microbiota profiling (QMP) on fecal samples, combining 16S rRNA gene sequencing with flow cytometric quantification of microbial cell counts[25].

The Bristol Stool Scale (BSS) was used to describe the consistency of each individual stool sample as a proxy of intestinal transit time. The proportion of abnormally hard stools (BSS 1-2) and loose stools (BSS 6-7) was similar between FD and HC (P = 0.81) (**Figure 4A**). Next, we assessed beta-diversity on the QMP matrix as a measure of compositional difference. Overall, both groups exhibited a similar fecal microbial composition as no separate clustering was observed using principal coordinate analysis (PCoA, Bray-Curtis dissimilarity) (**Figure 4B**). PERMANOVA confirmed the absence of a significant difference between groups (R^2 = 0.011, $P_{PERMANOVA}$ = 0.63). Stool consistency explained a significant proportion of compositional variance in this cohort (R^2 = 0.047, $P_{PERMANOVA}$ = 0.025) while controlling for study group and PPI intake (**Supplementary Figure 2A**), in line with previous reports[21, 26, 27]. Therefore, BSS was included as a covariate in downstream microbial analyses.

The variance in microbial counts between groups was similar (F = 1.11, P = 0.78), indicating that the individual microbiota of patients with FD were not extremely dense or depleted compared to HC (**Figure 4C**). Differential genera abundance analysis (prevalence cutoff of ≥ 20%, 68 bacterial genera), revealed a trend toward decreased *Odoribacter* (-0.68 ± 0.24), *Turicibacter* (-0.81 ± 0.28) and unclassified Clostridia (-1.11 ± 0.37, all q_{FDR} = 0.075) abundance, as well as increased *Flavonifractor* (0.77 ± 0.27, q_{FDR} = 0.075) abundance (**Figure 4D**, **Supplementary Results**, **Supplementary Table 9**). In summary, despite an overall similar fecal microbial composition, the quantitative abundance of select taxa was different in patients with FD. These shifts were independent of PPI intake and intestinal transit time, although transit time was linked with a higher number of differentially abundant fecal genera.

Specific taxa are associated with metabolite and symptom profiles

Even though the gut microbiota in FD closely resembled that of HC, we explored specific associations between the fecal microbiota and altered metabolite levels or symptomatology. First, PERMANOVA revealed a close association between fecal microbiota community variation and peripheral metabolite profiles, while controlling for intestinal transit time (BSS) (**Supplementary Results**, **Supplementary Table 10**). Next, we performed correlation analyses between the four differentially abundant bacterial genera in FD compared to HC with select metabolites and symptoms that were substantially different between the study groups.

Unclassified *Clostridia* were significantly and positively associated with various urinary and systemic AAA metabolites, but not with any of the symptom measures (**Figure 5A**, **Supplementary Table 11**). In contrast, no associations were found for *Flavonifractor*, *Odoribacter* and *Turicibacter* with any of the selected metabolite levels, nor with the included GI and extraintestinal symptoms (**Figure 5A**, **Supplementary Table 11**).

The prevalence of the four differentially abundant genera across all fecal samples in this cohort was 33% (25/76), 57% (43/76), 53% (40/76) and 32% (24/76), respectively. We next asked whether symptom profiles and metabolite levels were linked to any of the most abundant bacterial genera. To this end, we repeated the correlation analyses including the twenty most abundant bacterial genera and the same set of symptom and metabolite variables. Interestingly, a cluster consisting of *Anaerostipes* and *Fusicatenibacter* was strongly associated with a mild symptom profile, suggesting a beneficial role for these genera (**Figure 5B**, **Supplementary Table 12**). Reduced plasma propionate and total SCFA levels in FD tended to be associated with a lower fecal abundance of *Collinsella* and *Bifidobacterium* (**Figure 5B**, **Supplementary Table 12**). Microbial AAA metabolite concentrations were linked to a separate bacterial cluster containing *Clostridium IV* and unclustered *Ruminococcaceae*, while the association with *Clostridium IV* appeared to be driven by PAGln, both in serum and urine (**Figure 5B**, **Supplementary Table 12**). The differential abundance of host-derived AAA metabolites, as well as serum Kyn and Phe was not linked with specific fecal bacterial abundance, likely owing to their non-microbial origin (**Figure 5B**, **Supplementary Table 12**). Urinary IAA levels tended to correlate positively with fecal *Prevotella* abundance ($\rho = 0.34$, $q_{FDR} = 0.092$), but inversely with *Bacteroides* abundance ($\rho = -0.31$, $q_{FDR} = 0.092$) (**Figure 5B**, **Supplementary Table 12**). We could not test the previously reported association of IAA with *Lactobacillus* abundance[24] as this genus was only detected in less than 20% of the fecal samples. In summary, non-overlapping clusters of specific bacteria correlate separately with psychological symptoms and microbial metabolites. This suggests that the observed associations between select intestinal metabolites and the combined GI and extraintestinal symptom profile in FD do not share a mutual gut microbiota signature.

Resting-state functional connectivity in salience, emotional-arousal, and central autonomic brain networks is altered in FD and accurately classifies FD and HC

Gut microbiota metabolites have been proposed as important contributors to microbiota-gut-brain interplay, which is thought to be a major driver underlying disorders of gut-brain interactions such as FD. However, studies that comprehensively consider these gut microbiota, metabolite and brain components are scarce. Therefore, participants in this study

underwent optional resting-state functional magnetic resonance imaging (rs-fMRI) of the brain, completed by 27 patients with FD and 20 HC, supplemented with data from 16 additional HC who underwent identical rs-fMRI procedures. This cohort of 36 HC had a similar sex distribution compared to the 27 FD patients (25 females (69%) vs 22 females (81%), $P = 0.38$) but was on average younger (mean age (years) ± standard deviation age: 28 ± 9 years vs 34 ± 12, $P = 0.015$).

Multivariate general linear model (GLM) analyses on the region-of-interest (ROI)-to-ROI connectivity matrix including 44 a priori selected ROIs involved in salience, emotional-arousal and central autonomic networks[28], demonstrated a significant difference in connectivity between FD and HC for the right inferior frontal gyrus - pars triangularis (ventrolateral prefrontal cortex, vlPFC) (ROI mass = 61.27, $P = 0.0013$, $P_{FWE} = 0.046$). This was driven by significantly stronger connectivity with the bilateral rostral anterior cingulate cortex and gyrus rectus as well as with left medial fronto-orbital gyrus and superior frontal gyrus in FD versus HC (**Figure 6A**, **Supplementary Table 13**).

Next, we applied functional connectivity multivariate pattern analysis (fc-MVPA) as a whole-brain data-driven approach to identify regions in which connectivity with the rest of the brain differs between FD and HC. A significant between-group difference in whole-brain voxel-based connectivity was found for a cluster in the left vlPFC including frontal orbital cortex and inferior frontal gyrus - pars triangularis (peak MNI coordinates [x, y, z] = [-41, 33, -7]; k = 61 voxels; TFCE = 431.76; $P = 0.001$; $P_{FWE} = 0.048$) (**Figure 6B**). This difference was driven by stronger connectivity between this cluster and other (pre)frontal, inferior temporal, and cerebellar areas in FD patients (red), and stronger connectivity between this cluster and insular and parietal regions in HC (blue) (**Figure 6C**).

In addition to the differential pairwise connectivity relationships between groups, we applied graph theoretical analysis as a network-based approach and compared graph measures between FD and HC (FDR-corrected for 180 tests). Three out of the four global graph measures were significantly different between FD patients and HC ((M)ANOVA), with higher characteristic path length in HC, and higher efficiency and clustering coefficient in FD (**Supplementary Table 14**). For between-group analysis in nodal graph measures using (M)ANOVA, significant differences were found for characteristic path length in 30/44 ROIs, for betweenness centrality in 3/44 ROIs, for clustering coefficient in 20/44 ROIs, and for efficiency in 27/44 ROIs (**Supplementary Table 14**).

To test the collective ability of the calculated graph measures to discriminate between patients with FD and controls, they were entered as independent variables in partial least squares discriminant analysis (PLS-DA). PLS-DA with all 540 graph measures as X-variables and

group (FD versus HC) as Y-variable was performed and 5-fold cross-validation suggested a 2-factor solution with 63% of X-variables (339/540) exceeding the Variable Importance for Prediction (VIP) threshold of 0.8. The final model was run with these 339 X-variables and a 2-factor solution was again identified by the cross-validation procedure (van der Voet $T^2 = 0$, $Q^2 = 0.39$, cumulative $Q^2 = 0.69$) (**Supplementary Figure 3A**). The model cumulatively explained 34.7% and 76.0 % of the variance for the X-variables and the Y-variable, respectively, and 75% of X-variables (255/339) exceeded the VIP threshold of 0.8 (**Supplementary Table 15**). Classification performance was excellent, with only FD patient being misclassified as an HC (98% accuracy, 96% sensitivity, 100% specificity) (**Figure 6D**).

Altered resting-state functional brain connectivity mediates elevated urinary IAA levels in FD

Similarly, partial least squares (PLS) regression with all 540 graph measures as X-variables and urinary IAA as Y-variable was performed and leave-one-out cross-validation suggested a 2-factor solution with 59% of X-variables (320/540) exceeding the VIP threshold of 0.8. The final model was run with these 320 X-variables and a 2-factor solution was again identified by the cross-validation procedure (van der Voet $T^2 = 0$, $Q^2 = 0.51$, cumulative $Q^2 = 0.58$) (**Supplementary Figure 3B**). The model cumulatively explained 35.0 % and 83.3 % of the variance for the X-variables and the Y-variable, respectively, and 73% of X-variables (232/320) exceeded the VIP threshold of 0.8 (**Supplementary Table 16**). Moreover, the PLS regression model significantly predicted urinary IAA levels with near-perfect accuracy (Pearson $r = 0.91$, $P < 0.0001$) (**Supplementary Figure 3C**). In similar models with plasma propionate or serum Kyn as the Y-variable, the cross-validation procedure did not suggest any factors to retain (based on a minimum value for the root mean PRESS statistic for the null model), indicating that the X-variables (i.e. graph measures) did not explain any variance in the Y-variables (**Supplementary Figure 3D**).

Of note, one-way ANOVA revealed that the standardized first factor of the PLS regression model – explaining 19% of the variance in the graph measures – was significantly higher in FD ($\eta_p^2 = 0.23$, $P = 0.0011$), while the second factor (explaining 16% variance) was not different between groups ($\eta_p^2 = 0.013$, $P = 0.48$) (**Supplementary Figure 3E**). This prompted us to test whether the group difference in urinary IAA levels was mediated by differences in graph measures. For this purpose, we fitted a mediation model with group as the independent (X) variable, the standardized first graph measures factor of the PLS regression model predicting urinary IAA as the mediator (M) variable, and the standardized urinary IAA levels as the dependent (Y) variable. The indirect effect of group on IAA through the graph measures factor was significant ($\beta \pm SE = -0.064 \pm 0.024$; 95% bootstrapped CI = [-0.112, -0.024]) and the

direct effect of group on IAA (path C') turned non-significant (-0.049 ± 0.028, η_p^2 = 0.07, *P* = 0.089) whereas the total effect of group on IAA (path C) was significant (-0.113 ± 0.030, η_p^2 = 0.025, *P* = 0.0006) (**Figure 6E**), confirming that differences in brain-connectivity measures mediated the higher urinary IAA levels in FD.

Discussion

The bidirectional interplay between the gut microbiota and the central nervous system, known as the microbiota-gut-brain axis, is well established through preclinical and clinical studies[29-31]. Nevertheless, its role in DGBI including FD remains incompletely understood. Here, we provide novel evidence for dysregulated SCFA and tryptophan metabolism in FD in the absence of major microbial alterations, which was linked to a worsened GI and psychological symptom profile. Rs-fMRI-based analysis of functional connectivity between relevant brain regions involved in salience, emotional-arousal and central autonomic networks demonstrated significant differences between FD and HC. Moreover, the increase in urinary IAA, a microbial tryptophan metabolite, in patients with FD was statistically mediated by differential brain connectivity between FD and HC, pointing toward a brain-to-gut signaling pathway previously identified in rodents.

We identified a dysregulated metabolite signature in FD compared to HC, with a marked reduction in circulating kynurenine but increased urinary IAA levels. This suggests a shift in tryptophan metabolism from the host kynurenine pathway toward microbial indole production. Interestingly, *Lactobacillus murinus*-produced IAA has recently been demonstrated to relay psychological stress to the gut in mice, where it caused impaired stem cell differentiation. In patients with major depressive disorder (MDD), *Lactobacillus* abundance and fecal IAA levels were higher compared to controls[24]. In contrast, supplementation of IAA partially alleviated colitis in mice by restoring intestinal barrier function[32], suggesting differential effects of IAA depending on the inflammatory and genetic context or mouse model.

All major SCFA concentrations (acetate, butyrate and propionate) measured in the circulation and feces were numerically lower in FD compared to controls, with the reduction in systemic propionate levels being most pronounced and statistically significant. This finding is especially interesting given that SCFA – important products of microbial carbohydrate degradation – can influence central processes when reaching the systemic circulation[14]. Lower systemic SCFA levels are in line with recent findings of decreased circulating butyrate and propionate levels in patients with MDD[33], suggesting that limited SCFA availability is particularly linked with the central and psychological aspects of FD. In addition, higher plasma butyrate but not propionate levels at baseline could predict remission of MDD at follow-up, making SCFA attractive candidates to serve as prognostic, predictive, and/or therapeutic biomarkers in psychiatric disorders, and potentially DGBI including FD.

Importantly, altered metabolite levels in FD correlated with patient-reported outcomes, including two different measures of GI symptoms and various psychological outcomes such as anxiety, depression and extraintestinal symptom burden. This underscores the relevance of

metabolite dysregulation in FD, although cause and consequence cannot be untangled from our cross-sectional analysis. Indeed, whether an initial disruption of the gut microbiota leads to altered metabolite profiles in FD, or these gut disturbances are secondary to psychological cues such as elevated stress and anxiety, resulting in additional GI symptoms, will be a key next step in FD and DGBI research. Finding pathophysiological similarities with other DGBI such as IBS, or psychiatric disorders might shed additional light on the precise role of microbial and metabolite alterations in the onset of GI symptoms. To this end, the measurement of relevant metabolites from readily available samples (urine or blood) could inform clinicians on patient-tailored therapy selection (e.g. dietary and probiotic intervention over pharmacological intervention), paving the way for precision medicine in FD and related DGBI.

Despite significant shifts in metabolite profiles, we were unable to demonstrate major perturbations in the diversity and composition of the fecal microbiota in FD. Previous studies on microbial alterations in FD focused on the gastroduodenal environment, consistently demonstrating increased abundance of typical upper-GI bacteria such as *Streptococcus*[9, 10]. However, as microbial density and, consequently, the production of microbial metabolites progressively increase more distal to the duodenum, alterations in the composition of the lower GI microbiota might still be indirectly involved in gastroduodenal and psychological symptom generation. A recent case-control study from South-Korea in 12 patients with FD found an overall similar fecal microbiota composition compared to 16 controls as assessed by alpha and beta diversity[34], which we corroborated in a larger cohort with a different geographical origin. Relative abundances of *Butyricicoccus* and *Faecalibacterium* – known butyrate producers – were reduced in FD, which is in line with our findings of lower SCFA concentrations in general, and a decreased abundance of the SCFA-producing genus *Odoribacter*. Of note, inverse associations between fecal *Fusicatenibacter* abundance and various psychological symptoms including PTSD are consistent with a reduction in *Fusicatenibacter saccharivorans* in Spanish individuals with comorbid depression, anxiety and PTSD symptoms in the post-COVID-19 pandemic setting[35].

To the best of our knowledge, this is the first study to demonstrate a reduction in SCFA levels in FD compared to HC. Nevertheless, we and others reported on the beneficial effects of probiotics for FD in randomized placebo-controlled trials, associated with proliferation of SCFA-producing microbes. A combination of two spore-forming *Bacillus* strains (*B. coagulans* MY01 and *B. subtilis MY02*) effectively reduced FD symptoms and increased the fecal abundance of butyrate-producing genera *Faecalibacterium* and *Roseburia* after 8 and 16 weeks of probiotic intervention[36]. More recently, a Chinese study in 200 patients with FD demonstrated superior symptom relief of a high-dose probiotic consisting of *Bifidobacterium animalis* subsp. *lactis* BL-99 compared to various control groups (placebo, low-dose probiotic,

PPI treatment)[37]. Similarly, BL-99 probiotic intervention increased the abundance of multiple SCFA-producing microbes in stool, resulting in elevated fecal and systemic SCFA levels. This warrants further investigation on the anticipated beneficial effects of intervention with probiotics, as well as prebiotics, aimed at restoring circulating SCFA levels in randomized controlled trials.

One of the most intriguing findings of our study is the significantly altered brain connectivity in patients with FD compared to HC, which validates FD as a disorder of gut-brain interaction. Altered connectivity of the ventrolateral prefrontal cortex – a region implicated in reward valuation and pain modulation – with other emotional-arousal, salience, executive, and central autonomic network regions was found to be a unique brain feature in FD. Moreover, assessment of the global organization of brain connectivity networks through application of graph theoretical analysis pointed toward an overall altered network topology between FD and HC. This was further substantiated by a near-perfect classification of patients and controls based on this topological analysis. These findings corroborate the results from multiple studies that reported on functional brain alterations in FD (reviewed in[38-41]), supporting the concept that the pathogenesis of this disorder likely involves a combination of central and peripheral impairments. However, this study is the first to integrate brain connectivity measurements with microbial metabolite profiles – particularly the tryptophan metabolite IAA – in a translational hypothesis-driven fashion. Indeed, the graph measures partial least squares regression model explained a substantial portion of the variation in urinary IAA levels. Of note, brain connectivity was not linked to propionate or kynurenine concentrations, indicating a specific effect for IAA. Although causality cannot be inferred from this cross-sectional study, statistical mediation analysis suggested that elevated IAA might be driven by the observed brain connectivity changes in FD. In addition, this translates the preclinical findings by Wei *et al*. of increased IAA levels in various mouse models of psychological stress[24], to a human context of a disorder where psychological stress is thought to play an important role.

Some limitations inherent to the design of the study should be acknowledged. This study applied targeted metabolomics, measuring a limited number of AAA and their metabolites, leaving other potentially relevant metabolites unexplored. However, the targeted metabolomics approach ensured an optimized and validated analysis of several key tryptophan metabolites implicated in gut-brain communication, as well as the major SCFA, in multiple human samples. Our microbial analysis was conducted by 16S rRNA gene sequencing, which is limited in resolution and inference of microbial functionality. Future studies using metagenomic sequencing should focus on identifying the pathways underlying these observed metabolomic alterations. In the current study, fMRI was restricted to resting state measurements. Future studies using task-based imaging could identify alterations in connectivity and activity in

specific disorder-related contexts including stress, anxiety or pain. Lastly, findings from this relatively small single-center study should be confirmed in larger and diverse populations, controlling for the effects of geography and diet. Nevertheless, current metabolite analyses were adjusted for major dietary confounders including protein and fiber intake, as assessed by validated food frequency questionnaires.

Taken together, our study is the first to integrate peripheral microbiota-related alterations with central functionality in FD, adding to the growing body of evidence for a disturbed microbiota-gut-brain axis in FD. The first human data on alterations in tryptophan and short-chain fatty metabolism in FD – linked to its typical symptomatology – highlight their potential as prognostic, predictive, or therapeutic biomarkers for this condition. Moreover, they form a solid basis for the continued investigation of microbiota and metabolite modulation by dietary, probiotic or prebiotic intervention to target gut-brain alterations in this difficult-to-treat disorder.

Figure legends

Figure 1: High comorbid psychological symptom burden in FD. Between-group differences in gastrointestinal (LPDS, PAGI-SYM) and psychological (GAD7, VSI, PSQ9, PHQ12, PSS, PTSD, PANAS+, PANAS-) symptoms. Linear regression models with 'PPI intake' nested in the grouping variable. *P* values represent main group effects.

Figure 2: Patients with FD exhibit a distinct metabolite profile. (**A**) Aromatic amino acids (AAA) and AAA metabolites included in the targeted metabolomics approach. Tryptophan and its metabolites are underlined. Principal component analysis of (**B**) serum AAA and AAA metabolites, and (**C**) urinary microbial AAA metabolites. Permutational analysis of variance (PERMANOVA, 10,000 permutations) quantified explained proportion of variance (R^2) by 'Group'. Between-group differences in standardized concentrations of AAA and AAA metabolites aggregated per origin, measured in (**D**) serum and (**E**) urine, (**F**) and levels of selected individual AAA metabolites. Between-group differences in concentrations of short-chain fatty acids (SCFA) measured in (**G**) feces and (**H**) plasma. Linear regression with main 'Group' effect and 'PPI intake' nested in the grouping variable, adjusted for fiber (SCFA) or protein (AAA and AAA metabolites) intake. *P* values represent main 'Group' effects (**D**-**H**).

Figure 3: IAA, propionate and Kyn are associated with gastrointestinal and comorbid psychological symptoms in FD. (**A**) Heatmap of associations between symptom scores and metabolites. Color scale depicts Spearman correlation coefficients. Bonferroni-Holm adjusted significance depicted as open ($q_{FDR} < 0.1$) or filled circles ($q_{FDR} < 0.05$). Linear relationships between psychological (GAD7, PSQ9, PHQ12) and gastrointestinal (LPDS) symptom scores with (**B**) urinary indole-3-acetate (IAA), (**C**) plasma propionate, and (**D**) serum kynurenine (Kyn). (**E**) Heatmap of pairwise correlations between significantly altered metabolites of interest in FD. Color scale and values depict Spearman correlation coefficients. (**F**) Multiple linear regression analysis between significantly altered metabolites of interest in FD and symptom scores with correction for fiber and protein intake. Circle sizes correspond to Bonferroni-Holm adjusted *P* values (q_{FDR}). Color scale depicts effect sizes (η_p^2).

Figure 4: The fecal microbiota in FD is similar compared to HC and shaped by intestinal transit time. (**A**) Distribution of stool sample consistency types between FD and HC (Bristol Stool Scale, BSS). (**B**) Principal coordinate analysis (PCoA, Bray-Curtis) of fecal microbiota in FD and HC. Permutational analysis of variance (PERMANOVA, 10,000 permutations) quantified explained proportion of variance (R^2) by 'Group'. (**C**) Absolute abundance of ten most abundant fecal bacterial genera. (**D**) Univariable (between-group differences) and multivariable (between-group differences controlled for proton pump inhibitor (PPI) intake and intestinal transit time (BSS)) fecal microbial genera abundance analysis. Circle sizes

correspond to Bonferroni-Holm adjusted *P* values (q_{FDR}). Color scale depicts individual effect sizes.

Figure 5: Specific taxa are associated with metabolite and symptom profiles. Heatmap of associations between altered symptom scores and metabolites in FD with (**A**) differentially abundant fecal genera between FD and HC, and (**B**) twenty most abundant fecal genera. Color scale depicts Spearman correlation coefficients. Bonferroni-Holm adjusted significance depicted as open ($q_{FDR} < 0.1$) or filled circles ($q_{FDR} < 0.05$).

Figure 6: Resting-state functional brain connectivity is altered in FD and mediates elevated urinary IAA levels. (**A**) Between-group difference in region-of-interest (ROI)-to-ROI-based connectivity for the right inferior frontal gyrus (IFG) – pars triangularis (ventrolateral prefrontal cortex, vlPFC). (**B**) Between-group difference in whole-brain voxel-based connectivity for the left vlPFC (arrow). (**C**) Difference in connectivity pattern of the left vlPFC cluster with other brain regions between FD (red) and HC (blue). (**D**) Receiver operating characteristic (ROC) curve and area under the curve (AUC) depicting the performance of brain connectivity network partial least squares discriminant analysis (PLS-DA) classification between patients with FD and HC. (**E**) Mediation of between-group differences on urinary indole-3-acetate (IAA) levels. Introducing brain connectivity (resting-state functional magnetic resonance imaging (fMRI)-based graph measures factor 1) as mediator (significant between-group effect on brain connectivity (Path A) and association of brain connectivity with urinary IAA (Path B)) of the direct between-group effect on urinary IAA (Path C) eliminated the significance of the direct between-group effect on urinary IAA (Path C'). Model outcomes of the individual mediation paths are summarized as estimate (β) ± standard error (SE) with corresponding effect sizes (η_p^2). ** $P < 0.01$; *** $P < 0.001$.

Acknowledgements

The authors thank all the patients and volunteers for their participation in this study. We thank the personnel of the Endoscopy and Motility unit at the University Hospitals Leuven campus Gasthuisberg for their assistance with clinical study visits, in particular Karlien Geboers and Lieselot Holvoet. The authors thank Leen Rymenans, Chloë Verspecht and Thi Thuy Duyen Nguyen for their contribution to sample analysis. Icons in Figure 2B, Figure 2C, Supplementary Figure 1A and Supplementary Figure 1B were exported with license to publish from BioRender.com.

Conflict of interest

The authors disclose no conflicts.

Funding

M.C. is supported by a postdoctoral fellowship of the Belgian American Educational Foundation (BAEF). L.W. was supported by Flanders Research Foundation (FWO Vlaanderen) through a doctoral fellowship (1190619N). R.Y.T. and B.D are funded by a postdoctoral fellowship from the Research Fund–Flanders. A.V.V. is a postdoctoral researcher supported by a Marie-Curie grant (HORIZON-MSCA-2023). J.T. is supported by a KU Leuven Methusalem grant (EZX-C9725-METH/14/05). L.V.O. is a research professor of the KU Leuven Special Research Fund. T.V. is a senior clinical researcher supported by the Research Fund-Flanders (FWO, 1830517N), an FWO research grant (G059822N) and a grant from the Clinical Research Fund UZ Leuven (KOOR project financiering). The Raes lab is supported by KU Leuven, VIB and the Rega Institute. This study was supported by a grant of the Biocodex Microbiota Foundation (BMF Belux 2018) and a grant of the clinical research fund (KOOR) of the University Hospitals Leuven.

References

1. Stanghellini V, Chan FK, Hasler WL, et al. Gastroduodenal Disorders. Gastroenterology 2016;150:1380-92.
2. Sperber AD, Bangdiwala SI, Drossman DA, et al. Worldwide Prevalence and Burden of Functional Gastrointestinal Disorders, Results of Rome Foundation Global Study. Gastroenterology 2021;160:99-114.
3. Drossman DA, Hasler WL. Rome IV-functional GI disorders: disorders of gut-brain interaction. Gastroenterology 2016;150:1257-61.
4. Aro P, Talley NJ, Agréus L, et al. Functional dyspepsia impairs quality of life in the adult population. Aliment Pharmacol Ther 2011;33:1215-24.
5. Trindade IA, Hreinsson JP, Melchior C, et al. Global Prevalence of Psychological Distress and Comorbidity With Disorders of Gut-Brain Interactions. Am J Gastroenterol 2024;119:165-175.
6. Lacy BE, Weiser KT, Kennedy AT, et al. Functional dyspepsia: the economic impact to patients. Aliment Pharmacol Ther 2013;38:170-7.
7. Shah A, Fairlie T, Brown G, et al. Duodenal Eosinophils and Mast Cells in Functional Dyspepsia: A Systematic Review and Meta-Analysis of Case-Control Studies. Clin Gastroenterol Hepatol 2022;20:2229-2242.e29.
8. Vanheel H, Vicario M, Vanuytsel T, et al. Impaired duodenal mucosal integrity and low-grade inflammation in functional dyspepsia. Gut 2014;63:262-71.
9. Zhong L, Shanahan ER, Raj A, et al. Dyspepsia and the microbiome: time to focus on the small intestine. Gut 2017;66:1168-9.
10. Fukui A, Takagi T, Naito Y, et al. Higher levels of Streptococcus in upper gastrointestinal mucosa associated with symptoms in patients with functional dyspepsia. Digestion 2020;101:38-45.
11. Shanahan ER, Kang S, Staudacher H, et al. Alterations to the duodenal microbiota are linked to gastric emptying and symptoms in functional dyspepsia. Gut 2023;72:929-938.
12. Wauters L, Tito RY, Ceulemans M, et al. Duodenal Dysbiosis and Relation to the Efficacy of Proton Pump Inhibitors in Functional Dyspepsia. Int J Mol Sci 2021;22.
13. Jones MP, Tack J, Van Oudenhove L, et al. Mood and Anxiety Disorders Precede Development of Functional Gastrointestinal Disorders in Patients but Not in the Population. Clin Gastroenterol Hepatol 2017;15:1014-1020.e4.
14. Dalile B, Van Oudenhove L, Vervliet B, et al. The role of short-chain fatty acids in microbiota-gut-brain communication. Nat Rev Gastroenterol Hepatol 2019;16:461-478.

15. Gheorghe CE, Martin JA, Manriquez FV, et al. Focus on the essentials: tryptophan metabolism and the microbiome-gut-brain axis. Curr Opin Pharmacol 2019;48:137-145.
16. Matthys C, Meulemans A, Schueren BVd. Development and validation of general FFQ for use in clinical practice. Ann Nutr Metab 2015;67:239-239.
17. Lewis SJ, Heaton KW. Stool form scale as a useful guide to intestinal transit time. Scand J Gastroenterol 1997;32:920-4.
18. de Loor H, Poesen R, De Leger W, et al. A liquid chromatography - tandem mass spectrometry method to measure a selected panel of uremic retention solutes derived from endogenous and colonic microbial metabolism. Anal Chim Acta 2016;936:149-56.
19. Dalile B, Vervliet B, Bergonzelli G, et al. Colon-delivered short-chain fatty acids attenuate the cortisol response to psychosocial stress in healthy men: a randomized, placebo-controlled trial. Neuropsychopharmacology 2020;45:2257-2266.
20. Powers L, Osborn MK, Yang D, et al. Assay of the concentration and stable isotope enrichment of short-chain fatty acids by gas chromatography/mass spectrometry. Journal of Mass Spectrometry 1995;30:747-754.
21. Tito RY, Verbandt S, Aguirre Vazquez M, et al. Microbiome confounders and quantitative profiling challenge predicted microbial targets in colorectal cancer development. Nat Med 2024;30:1339-1348.
22. Tito RY, Chaffron S, Caenepeel C, et al. Population-level analysis of Blastocystis subtype prevalence and variation in the human gut microbiota. Gut 2019;68:1180-1189.
23. Wauters L, Ceulemans M, Frings D, et al. Proton pump inhibitors reduce duodenal eosinophilia, mast cells and permeability in patients with functional dyspepsia. Gastroenterology 2021;160:1521-31.
24. Wei W, Liu Y, Hou Y, et al. Psychological stress-induced microbial metabolite indole-3-acetate disrupts intestinal cell lineage commitment. Cell Metab 2024;36:466-483.e7.
25. Vandeputte D, Kathagen G, D'Hoe K, et al. Quantitative microbiome profiling links gut community variation to microbial load. Nature 2017;551:507-511.
26. Falony G, Joossens M, Vieira-Silva S, et al. Population-level analysis of gut microbiome variation. Science 2016;352:560-4.
27. Vandeputte D, Falony G, Vieira-Silva S, et al. Stool consistency is strongly associated with gut microbiota richness and composition, enterotypes and bacterial growth rates. Gut 2016;65:57-62.
28. Oishi K, Faria A, Jiang H, et al. Atlas-based whole brain white matter analysis using large deformation diffeomorphic metric mapping: application to normal elderly and Alzheimer's disease participants. Neuroimage 2009;46:486-99.

29. Collins SM, Surette M, Bercik P. The interplay between the intestinal microbiota and the brain. Nat Rev Microbiol 2012;10:735-42.
30. Mayer EA, Tillisch K, Gupta A. Gut/brain axis and the microbiota. J Clin Invest 2015;125:926-38.
31. Cryan JF, Dinan TG. Mind-altering microorganisms: the impact of the gut microbiota on brain and behaviour. Nat Rev Neurosci 2012;13:701-12.
32. Li M, Ding Y, Wei J, et al. Gut microbiota metabolite indole-3-acetic acid maintains intestinal epithelial homeostasis through mucin sulfation. Gut Microbes 2024;16:2377576.
33. Schiweck C, Dalile B, Balliet A, et al. Circulating short chain fatty acids are associated with depression severity and predict remission from major depressive disorder. Brain Behav Immun Health 2025;48:101070.
34. Kim SH, Choi Y, Oh J, et al. Associations among the Duodenal Ecosystem, Gut Microbiota, and Nutrient Intake in Functional Dyspepsia. Gut Liver 2024;18:621-631.
35. Malan-Müller S, Valles-Colomer M, Palomo T, et al. The gut-microbiota-brain axis in a Spanish population in the aftermath of the COVID-19 pandemic: microbiota composition linked to anxiety, trauma, and depression profiles. Gut Microbes 2023;15:2162306.
36. Wauters L, Slaets H, De Paepe K, et al. Efficacy and safety of spore-forming probiotics in the treatment of functional dyspepsia: a pilot randomised, double-blind, placebo-controlled trial. Lancet Gastroenterol Hepatol 2021;6:784-792.
37. Zhang Q, Li G, Zhao W, et al. Efficacy of Bifidobacterium animalis subsp. lactis BL-99 in the treatment of functional dyspepsia: a randomized placebo-controlled clinical trial. Nat Commun 2024;15:227.
38. Kano M, Dupont P, Aziz Q, et al. Understanding Neurogastroenterology From Neuroimaging Perspective: A Comprehensive Review of Functional and Structural Brain Imaging in Functional Gastrointestinal Disorders. J Neurogastroenterol Motil 2018;24:512-527.
39. Lee IS, Wang H, Chae Y, et al. Functional neuroimaging studies in functional dyspepsia patients: a systematic review. Neurogastroenterol Motil 2016;28:793-805.
40. Mao Y, Zhang P, Sun R, et al. Altered resting-state brain activity in functional dyspepsia patients: a coordinate-based meta-analysis. Front Neurosci 2023;17:1174287.
41. Sun R, Zhou J, Qu Y, et al. Resting-state functional brain alterations in functional dyspepsia: Protocol for a systematic review and voxel-based meta-analysis. Medicine (Baltimore) 2020;99:e23292.

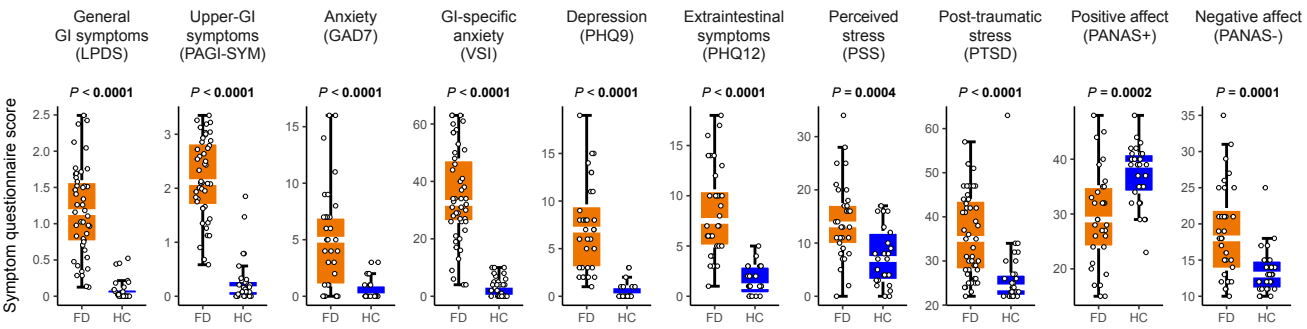
General GI symptoms (LPDS)
Upper-GI symptoms (PAGI-SYM)
Anxiety (GAD7)
GI-specific anxiety (VSI)
Depression (PHQ9)
Extraintestinal symptoms (PHQ12)
Perceived stress (PSS)
Post-traumatic stress (PTSD)
Positive affect (PANAS+)
Negative affect (PANAS-)
Symptom questionnaire score
P < 0.0001
P < 0.0001
P < 0.0001
P < 0.0001
P < 0.0001
P < 0.0001
P = 0.0004
P < 0.0001
P = 0.0002
P = 0.0001
FD
HC

A

Molecule	Type
Phenylalanine (Phe)	Aromatic amino acids (AAA)
Tyrosine (Tyr)	
Tryptophan (Trp)	
p-Cresyl glucuronide (pCG)	Microbial AAA metabolites
p-Cresyl sulfate (pCS)	
Phenyl glucuronide (PhG)	
Phenyl sulfate (PhS)	
Phenylacetylglutamine (PAGln)	
Indole-3-acetate (IAA)	
Indoxyl sulfate (IxS)	
Hippuric acid (HA)	
Kynurenine (Kyn)	Host AAA metabolites
Kynurenic acid (KA)	
Trimethylamine N-oxide (TMAO)	Miscellaneous metabolites
3-carboxy-4-methyl-5-propyl-2-furanpropanoic acid (CMPF)	

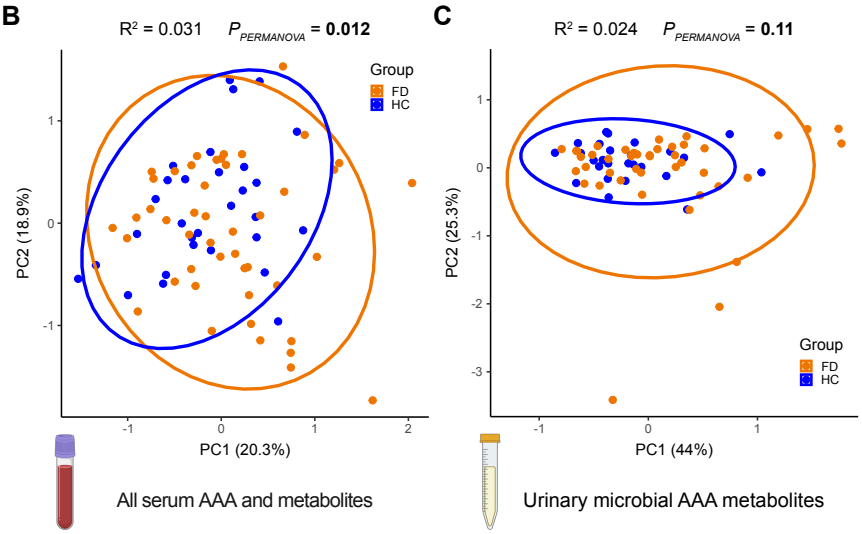

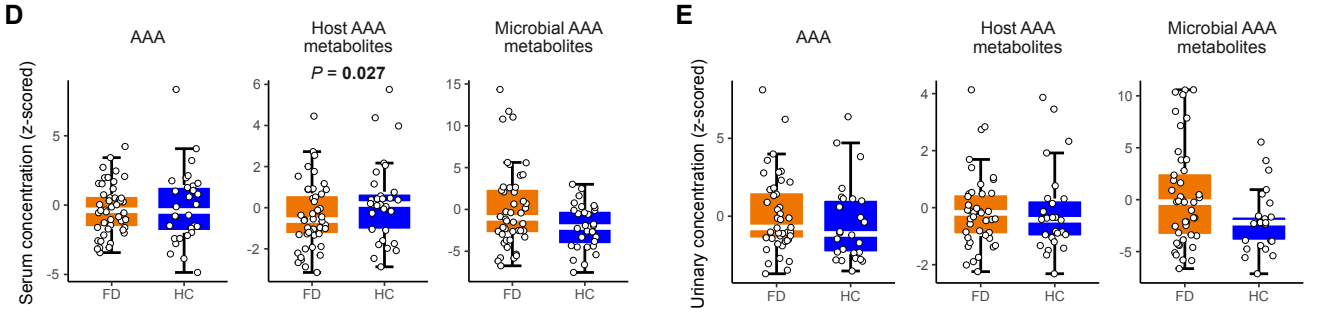

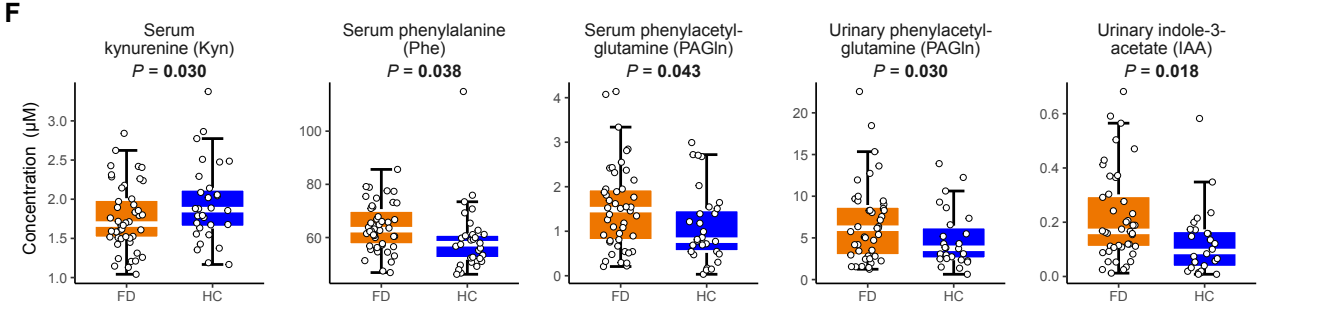

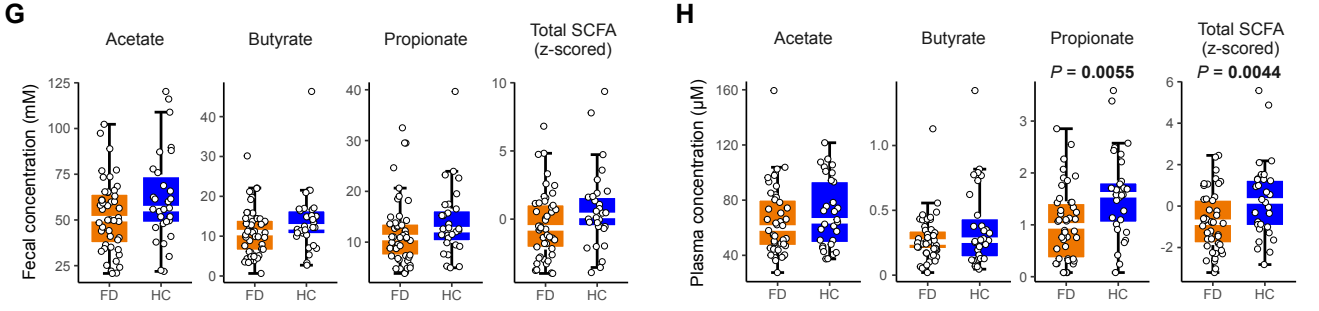

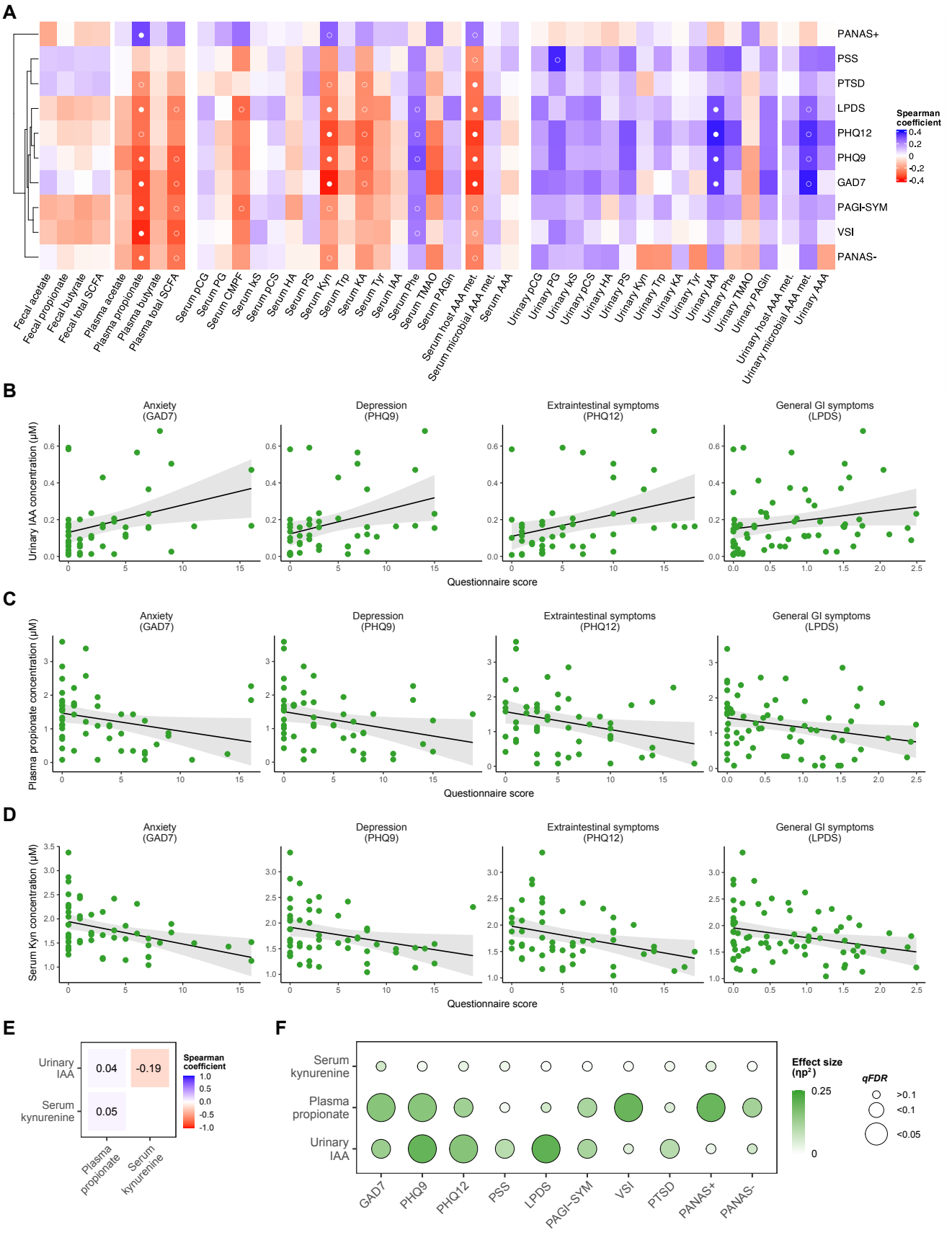
A
PANAS+
PSS
PTSD
LPDS
PHQ12
PHQ9
GAD7
PAGI-SYM
VSI
PANAS-
Spearman coefficient
0.4
0.2
0
-0.2
-0.4
Fecal acetate
Fecal propionate
Fecal butyrate
Fecal total SCFA
Plasma acetate
Plasma propionate
Plasma butyrate
Plasma total SCFA
Serum pCG
Serum PG
Serum CMPF
Serum kS
Serum pCS
Serum HA
Serum PS
Serum Kyn
Serum Trp
Serum KA
Serum Tyr
Serum IAA
Serum Phe
Serum TMAO
Serum PAGln
Serum host AAA met.
Serum microbial AAA met.
Serum AAA
Urinary pCG
Urinary PG
Urinary kS
Urinary pCS
Urinary HA
Urinary PS
Urinary Kyn
Urinary Trp
Urinary KA
Urinary Tyr
Urinary IAA
Urinary Phe
Urinary TMAO
Urinary PAGln
Urinary host AAA met.
Urinary microbial AAA met.
Urinary AAA
B
Anxiety (GAD7)
Depression (PHQ9)
Extraintestinal symptoms (PHQ12)
General GI symptoms (LPDS)
Urinary IAA concentration (μM)
Questionnaire score
C
Anxiety (GAD7)
Depression (PHQ9)
Extraintestinal symptoms (PHQ12)
General GI symptoms (LPDS)
Plasma propionate concentration (μM)
Questionnaire score
D
Anxiety (GAD7)
Depression (PHQ9)
Extraintestinal symptoms (PHQ12)
General GI symptoms (LPDS)
Serum Kyn concentration (μM)
Questionnaire score
E
Urinary IAA
Serum kynurenine
0.04
-0.19
0.05
Plasma propionate
Serum kynurenine
Spearman coefficient
1.0
0.5
0.0
-0.5
-1.0
F
Serum kynurenine
Plasma propionate
Urinary IAA
GAD7
PHQ9
PHQ12
PSS
LPDS
PAGI-SYM
VSI
PTSD
PANAS+
PANAS-
Effect size (np²)
0.25
0
qFDR
>0.1
<0.1
<0.05

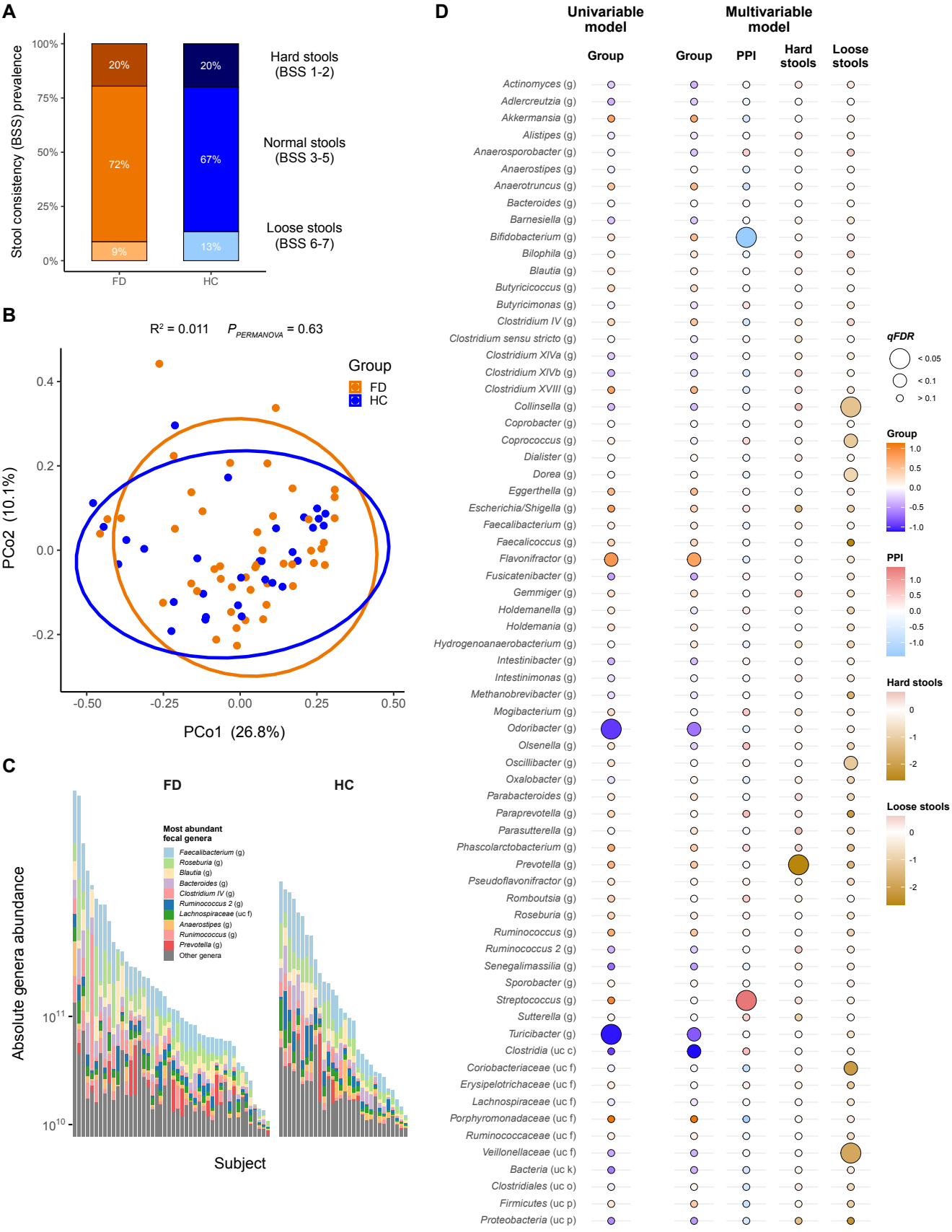
A
Stool consistency (BSS) prevalence
100%
75%
50%
25%
0%
20%
72%
9%
20%
67%
13%
FD
HC
Hard stools (BSS 1-2)
Normal stools (BSS 3-5)
Loose stools (BSS 6-7)
B
R² = 0.011 P PERMANOVA = 0.63
Group
FD
HC
PCo2 (10.1%)
PCo1 (26.8%)
0.4
0.2
0.0
-0.2
-0.50
-0.25
0.00
0.25
0.50
C
FD
HC
Absolute genera abundance
Most abundant fecal genera
Faecalibacterium (g)
Roseburia (g)
Blautia (g)
Bacteroides (g)
Clostridium IV (g)
Ruminococcus 2 (g)
Lachnospiraceae (uc f)
Anaerostipes (g)
Runimococcus (g)
Prevotella (g)
Other genera
10^11
10^10
Subject
D
Univariable model
Multivariable model
Group
Group
PPI
Hard stools
Loose stools
Actinomyces (g)
Adlercreutzia (g)
Akkermansia (g)
Alistipes (g)
Anaerosporobacter (g)
Anaerostipes (g)
Anaerotruncus (g)
Bacteroides (g)
Barnesiella (g)
Bifidobacterium (g)
Bilophila (g)
Blautia (g)
Butyricicoccus (g)
Butyricimonas (g)
Clostridium IV (g)
Clostridium sensu stricto (g)
Clostridium XIVa (g)
Clostridium XIVb (g)
Clostridium XVIII (g)
Collinsella (g)
Coprobacter (g)
Coprococcus (g)
Dialister (g)
Dorea (g)
Eggerthella (g)
Escherichia/Shigella (g)
Faecalibacterium (g)
Faecalicoccus (g)
Flavonifractor (g)
Fusicatenibacter (g)
Gemmiger (g)
Holdemanella (g)
Holdemania (g)
Hydrogenoanaerobacterium (g)
Intestinibacter (g)
Intestinimonas (g)
Methanobrevibacter (g)
Mogibacterium (g)
Odoribacter (g)
Olsenella (g)
Oscillibacter (g)
Oxalobacter (g)
Parabacteroides (g)
Paraprevotella (g)
Parasutterella (g)
Phascolarctobacterium (g)
Prevotella (g)
Pseudoflavonifractor (g)
Romboutsia (g)
Roseburia (g)
Ruminococcus (g)
Ruminococcus 2 (g)
Senegalimassilia (g)
Sporobacter (g)
Streptococcus (g)
Sutterella (g)
Turicibacter (g)
Clostridia (uc c)
Coriobacteriaceae (uc f)
Erysipelotrichaceae (uc f)
Lachnospiraceae (uc f)
Porphyromonadaceae (uc f)
Ruminococcaceae (uc f)
Veillonellaceae (uc f)
Bacteria (uc k)
Clostridiales (uc o)
Firmicutes (uc p)
Proteobacteria (uc p)
qFDR
< 0.05
< 0.1
> 0.1
Group
1.0
0.5
0.0
-0.5
-1.0
PPI
1.0
0.5
0.0
-0.5
-1.0
Hard stools
0
-1
-2
Loose stools
0
-1
-2

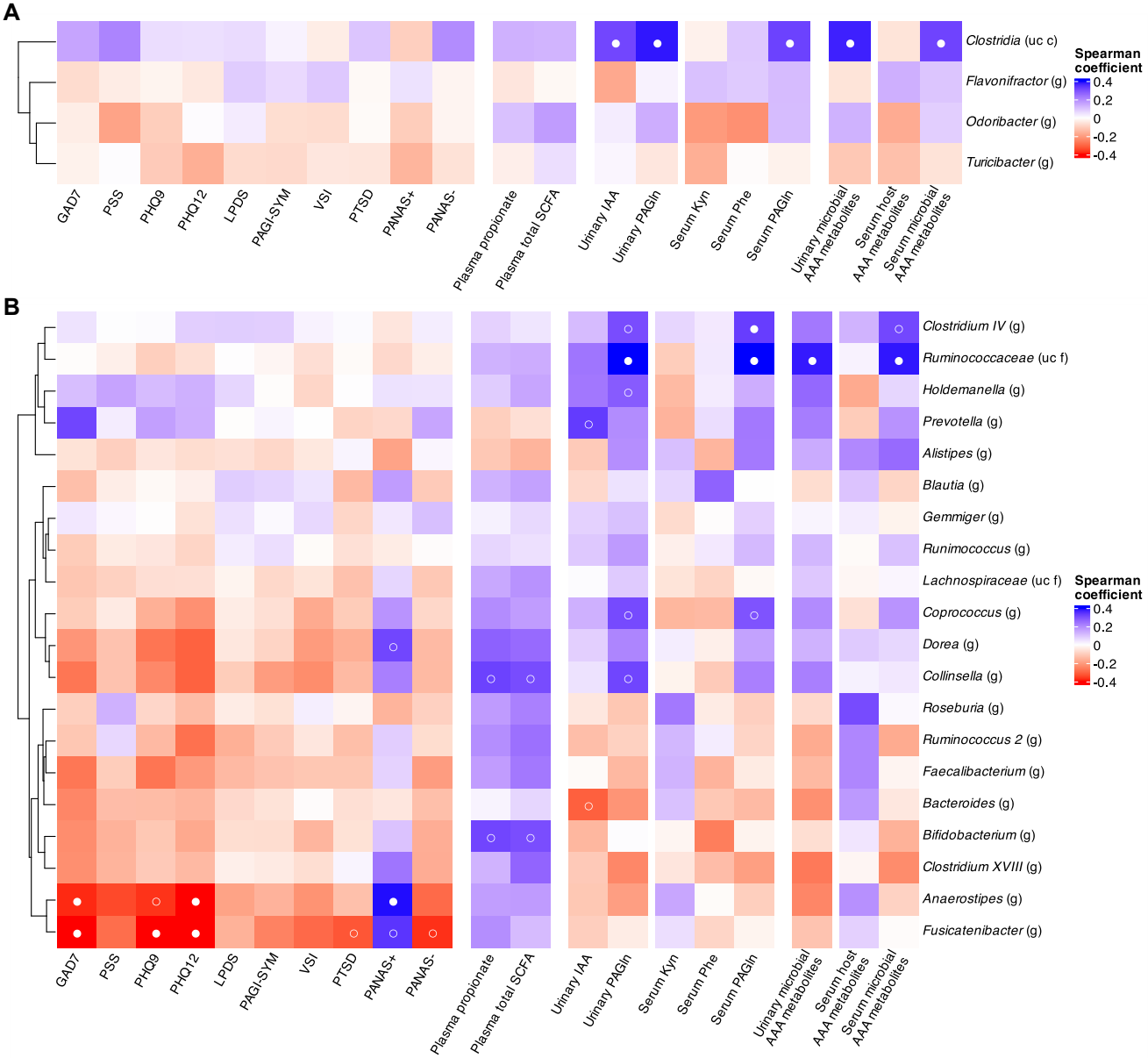
A
Clostridia (uc c)
Flavonifractor (g)
Odoribacter (g)
Turicibacter (g)
Spearman coefficient
0.4
0.2
0
-0.2
-0.4
GAD7
PSS
PHQ9
PHQ12
LPDS
PAGI-SYM
VSI
PTSD
PANAS+
PANAS-
Plasma propionate
Plasma total SCFA
Urinary IAA
Urinary PAGln
Serum Kyn
Serum Phe
Serum PAGln
Urinary microbial AAA metabolites
Serum host AAA metabolites
Serum microbial AAA metabolites
B
Clostridium IV (g)
Ruminococcaceae (uc f)
Holdemanella (g)
Prevotella (g)
Alistipes (g)
Blautia (g)
Gemmiger (g)
Runimococcus (g)
Lachnospiraceae (uc f)
Coprococcus (g)
Dorea (g)
Collinsella (g)
Roseburia (g)
Ruminococcus 2 (g)
Faecalibacterium (g)
Bacteroides (g)
Bifidobacterium (g)
Clostridium XVIII (g)
Anaerostipes (g)
Fusicatenibacter (g)
Spearman coefficient
0.4
0.2
0
-0.2
-0.4
GAD7
PSS
PHQ9
PHQ12
LPDS
PAGI-SYM
VSI
PTSD
PANAS+
PANAS-
Plasma propionate
Plasma total SCFA
Urinary IAA
Urinary PAGln
Serum Kyn
Serum Phe
Serum PAGln
Urinary microbial AAA metabolites
Serum host AAA metabolites
Serum microbial AAA metabolites

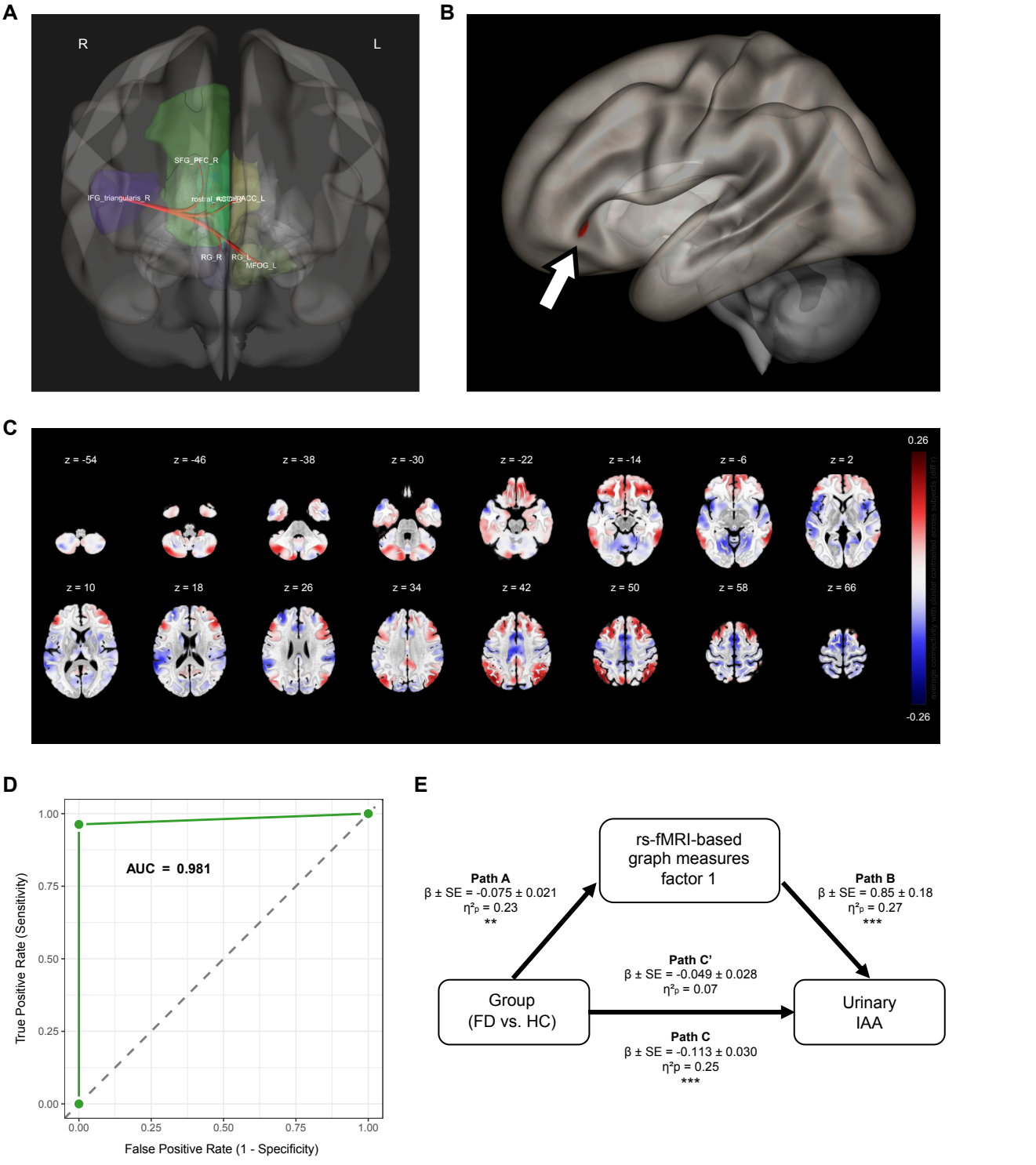
A
R
L
SFG_PFC_R
IFG_triangularis_R
rostral_ACC_R
RACC_L
RG_R
RG_L
MFOG_L
B
C
z = -54
z = -46
z = -38
z = -30
z = -22
z = -14
z = -6
z = 2
z = 10
z = 18
z = 26
z = 34
z = 42
z = 50
z = 58
z = 66
0.26
-0.26
D
AUC = 0.981
True Positive Rate (Sensitivity)
False Positive Rate (1 - Specificity)
1.00
0.75
0.50
0.25
0.00
E
rs-fMRI-based graph measures factor 1
Path A
β ± SE = -0.075 ± 0.021
η²p = 0.23
**
Path B
β ± SE = 0.85 ± 0.18
η²p = 0.27
***
Path C'
β ± SE = -0.049 ± 0.028
η²p = 0.07
Group (FD vs. HC)
Urinary IAA
Path C
β ± SE = -0.113 ± 0.030
η²p = 0.25
***

Supplementary methods

Study participants

Patients with FD were men or women between 18 and 64 years old who fulfilled the Rome IV criteria for FD[1]. Exclusion criteria were the presence of an active psychiatric, inflammatory or metabolic disorder. Structural alterations of the upper GI tract were excluded during upper GI endoscopy. Routine histological analysis of duodenal biopsies confirmed the normal appearance of the duodenal mucosa. All patients had a documented gastric biopsy to rule out *Helicobacter pylori* infection. Patient's medication intake was recorded and PPI intake at the time of sampling was defined as at least one month of one or more daily doses of any PPI before sampling. Healthy volunteers – men or women between 18 and 64 without any GI, psychiatric, inflammatory or metabolic disorder – were recruited as controls through advertisement. Participants did not use antibiotics or immunosuppressants within three months before sampling. Participants refrained from smoking and alcohol use within two days before sampling.

Symptom assessment

Gastrointestinal symptoms were assessed by the Patient Assessment of Upper GI Symptom Severity (PAGI-SYM)[2] and Leuven Postprandial Distress Scale (LPDS)[3]. Extraintestinal and psychological symptoms were assessed by the Generalized Anxiety Disorder-7 questionnaire (GAD7)[4], Patient Health Questionnaire-9 (PHQ9)[5], Perceived Stress Scale (PSS)[6], Visceral Sensitivity Index (VSI)[7], Post-Traumatic Stress Disorder (PTSD)[8], Childhood Trauma Questionnaire (CTQ)[9], Positive and Negative Affect Schedule (PANAS)[10], and the shortened PHQ15 questionnaire without GI-specific symptoms to evaluate extraintestinal symptom reporting (PHQ12)[11].

Fecal microbiota analysis

Quantitative microbiota profiling was performed by sequencing the V4 region of the 16S rRNA gene using the 515F (GTGYCAGCMGCCGCGGTAA) and 806R (GGACTACNVGGGTWTCTAAT) primer pair on the Illumina MiSeq platform (MiSeq Reagent Kit v2, 500 cycles, 15.38 % PhiX, 2 × 250 paired-end reads) at the VIB Nucleomics core laboratory (Leuven, Belgium). All fecal samples were processed in batch at the end of the study. The microbial load of frozen fecal samples was determined by flow cytometry on diluted fecal suspensions as detailed previously[12]. Microbial counts were determined using an Accuri C6 flow cytometer coupled to Accuri CSampler software (BD) with constant instrument and gating settings for all samples, as previously described[12, 13]. R (v4.4.1) was used for

bioinformatics analyses, applying the LotuS[14] and DADA2 (v1.6) pipelines[15]. The QMP matrix was built as described previously[12]. In brief, samples were rarefied to an even sampling depth, defined as the ratio between sampling size (16S rRNA gene copy number-corrected sequencing depth) and microbial load per sample (cell count per gram of frozen fecal material). A minimum rarefied read count of 150 was used and rarefied genus abundances were converted into numbers of cells per gram.

Functional magnetic resonance imaging

Preprocessing

Results included in this manuscript come from preprocessing performed using *fMRIPrep* 20.0.6 (RRID:SCR_016216)[16], which is based on *Nipype* 1.4.2 (RRID:SCR_002502)[17].

Anatomical data preprocessing

The T1-weighted (T1w) image was corrected for intensity non-uniformity (INU) with N4BiasFieldCorrection[18], distributed with ANTs 2.2.0 (RRID:SCR_004757)[19], and used as T1w-reference throughout the workflow. The T1w-reference was then skull-stripped with a *Nipype* implementation of the antsBrainExtraction.sh workflow (from ANTs), using OASIS30ANTs as target template. Brain tissue segmentation of cerebrospinal fluid (CSF), white-matter (WM) and gray-matter (GM) was performed on the brain-extracted T1w using fast (FSL 5.0.9, RRID:SCR_002823)[20]. Volume-based spatial normalization to one standard space (MNI152NLin2009cAsym) was performed through nonlinear registration with antsRegistration (ANTs 2.2.0), using brain-extracted versions of both T1w reference and the T1w template. The following template was selected for spatial normalization: *ICBM 152 Nonlinear Asymmetrical template version 2009c* (RRID:SCR_008796; TemplateFlow ID: MNI152NLin2009cAsym)[21].

Functional data preprocessing

For each of the 1 BOLD runs found per subject (across all tasks and sessions), the following preprocessing was performed. First, a reference volume and its skull-stripped version were generated using a custom methodology of *fMRIPrep*. Susceptibility distortion correction (SDC) was omitted. The BOLD reference was then co-registered to the T1w reference using flirt (FSL 5.0.9)[22] with the boundary-based registration[23] cost-function. Co-registration was configured with nine degrees of freedom to account for distortions remaining in the BOLD reference. Head-motion parameters with respect to the BOLD reference (transformation matrices, and six corresponding rotation and translation parameters) are estimated before any spatiotemporal filtering using mcflirt (FSL 5.0.9)[24]. BOLD runs were slice-time corrected using 3dTshift from AFNI 20160207 (RRID:SCR_005927)[25]. The BOLD time-series (including slice-timing

correction when applied) were resampled onto their original, native space by applying the transforms to correct for head-motion. These resampled BOLD time-series will be referred to as *preprocessed BOLD in original space*, or just *preprocessed BOLD*. The BOLD time-series were resampled into standard space, generating a *preprocessed BOLD run in MNI152NLin2009cAsym space*. First, a reference volume and its skull-stripped version were generated using a custom methodology of *fMRIPrep*. Several confounding time-series were calculated based on the *preprocessed BOLD*: framewise displacement (FD), DVARS and three region-wise global signals. FD and DVARS are calculated for each functional run, both using their implementations in *Nipype* (following the definitions by Power et al.[26]). The three global signals are extracted within the CSF, the WM, and the whole-brain masks. Additionally, a set of physiological regressors were extracted to allow for component-based noise correction (*CompCor*)[27]. Principal components are estimated after high-pass filtering the *preprocessed BOLD* time-series (using a discrete cosine filter with 128s cut-off) for the two *CompCor* variants: temporal (tCompCor) and anatomical (aCompCor). tCompCor components are then calculated from the top 5% variable voxels within a mask covering the subcortical regions. This subcortical mask is obtained by heavily eroding the brain mask, which ensures it does not include cortical GM regions. For aCompCor, components are calculated within the intersection of the aforementioned mask and the union of CSF and WM masks calculated in T1w space, after their projection to the native space of each functional run (using the inverse BOLD-to-T1w transformation). Components are also calculated separately within the WM and CSF masks. For each CompCor decomposition, the *k* components with the largest singular values are retained, such that the retained components' time series are sufficient to explain 50 percent of variance across the nuisance mask (CSF, WM, combined, or temporal). The remaining components are dropped from consideration. The head-motion estimates calculated in the correction step were also placed within the corresponding confounds file. The confound time series derived from head motion estimates and global signals were expanded with the inclusion of temporal derivatives and quadratic terms for each[28]. Frames that exceeded a threshold of 0.5 mm FD or 3.0 standardised DVARS were annotated as motion outliers. Four participants (two patients, two controls) were excluded due to excess head movement based on the criterion of >10% motion outliers. All resamplings can be performed with *a single interpolation step* by composing all the pertinent transformations (i.e. head-motion transform matrices, susceptibility distortion correction when available, and co-registrations to anatomical and output spaces). Gridded (volumetric) resamplings were performed using antsApplyTransforms (ANTs), configured with Lanczos interpolation to minimize the smoothing effects of other kernels[29]. Non-gridded (surface) resamplings were performed using mri_vol2surf (FreeSurfer).

Many internal operations of *fMRIPrep* use *Nilearn* 0.6.2 (RRID:SCR_001362)[30], mostly within the functional processing workflow. For more details of the pipeline, see the section corresponding to workflows in *fMRIPrep*'s documentation[31].

Finally, functional data were smoothed using spatial convolution with a Gaussian kernel of 8 mm full width half maximum (FWHM) using CONN (RRID:SCR_009550)[32] release 20.b and SPM[33] (RRID:SCR_007037) release 12.7771.

Denoising

Using CONN (RRID:SCR_009550)[32] release 20.b and SPM[33] (RRID:SCR_007037) release 12.7771, functional data were denoised using a standard denoising pipeline including the regression of potential confounding effects characterized by white matter timeseries (5 CompCor noise components), CSF timeseries (5 CompCor noise components), motion parameters and their first order derivatives (12 factors), outlier scans (below 37 factors), session effects and their first order derivatives (2 factors), and linear trends (2 factors) within each functional run, followed by bandpass frequency filtering of the BOLD timeseries between 0.008 Hz and 0.09 Hz. CompCor noise components within white matter and CSF were estimated by computing the average BOLD signal as well as the largest principal components orthogonal to the BOLD average, motion parameters, and outlier scans within each subject's eroded segmentation masks. From the number of noise terms included in this denoising strategy, the effective degrees of freedom of the BOLD signal after denoising were estimated to range from 77.7 to 89.9 (average 88.8) across all subjects.

ROI-to-ROI connectivity analysis

Multivariate GLM

ROIs

44 ROIs from the salience, emotional-arousal and central autonomic networks from the Johns Hopkins University atlas[34] (imported into CONN) based on 1) their hypothesized key role in DGBI according to a recent Rome working team report[35], 2) previous resting-state fMRI studies in FD, including systematic reviews and meta-analyses[36-44].

First-level analysis

ROI-to-ROI connectivity (RRC) matrices were estimated characterizing the functional connectivity between each pair of regions among 44 ROIs. Functional connectivity strength was represented by Fisher-transformed bivariate correlation coefficients from a general linear model (weighted-GLM[1]), estimated separately for each pair of ROIs, characterizing the

association between their BOLD signal timeseries. In order to compensate for possible transient magnetization effects at the beginning of each run, individual scans were weighted by a step function convolved with an SPM canonical hemodynamic response function and rectified.

Second-level analyses

Group-level analyses were performed using a General Linear Model (GLM). For each individual connection a separate GLM was estimated, with first-level connectivity measures at this connection as dependent variables (one independent sample per subject), and group as independent variable. Connection-level hypotheses were evaluated using multivariate parametric statistics with random-effects across subjects and sample covariance estimation across multiple measurements. Inferences were performed at the level of individual ROIs. ROI-level inferences were based on parametric multivariate statistics, combining the connection-level statistics across all connections from each individual ROI. Results were thresholded using a familywise corrected p-FWE < 0.05 ROI-level threshold (ROI mass/intensity).

Graph Theoretical Analysis

Graph Theoretical Analysis were performed using the GraphVar Toolbox[45, 46] version 2.03a. First, functional connectivity networks (i.e. ROI-to-ROI connectivity matrices) were constructed using the Group Sparse Representation method[47], a multi-region rather than pairwise-based network construction method shown to suppress spurious correlation and developed to improve performance in classification models, as implemented in the BrainNetClass toolbox[48] and built into GraphVar. These raw matrices served as inputs (relative thresholding at 0.3, 0.35, 0.4, 0.45, and 0.5 density thresholds) to calculate the following undirected global graph measures: assortativity (global), betweenness centrality (nodal), efficiency (global and nodal), characteristic path length (global and nodal), and clustering coefficient (global and nodal).

Graph measures were compared between FD patients and HC using a series of one-way ANOVAs (for non-density-dependent graph measures) and MANOVAs with density as repeatedly measured factor and the main effect of group (across densities) as the effect of interest for density-dependent graph measures in JMP® 18.2.1 software (JMP Statistical Discovery LLC, Cary, NC). The entire set of 180 resulting p-values was corrected for multiple testing using the positive FDR (q_{FDR}) option implemented in SAS 9.4 (TS1M7) proc multtest[49, 50].

To test the collective ability of the calculated graph measures to discriminate between FD patients and HC, they were entered as independent variables in Partial Least Squares (PLS) Discriminant Analysis using the nonlinear iterative partial least squares (NIPALS) method

implemented in JMP® 18.2.1 software (JMP Statistical Discovery LLC, Cary, NC) as it performs well in cases where the number of X values exceeds the number of observations and where X values may be strongly correlated because it reduces the dimensionality of the X-variables by a more limited number of latent factors. Five-fold cross-validation was used to determine the optimal number of factors and avoid overfitting the data, based on a combination of minimum root mean PRESS and Van der Voet T^2 statistics as well as maximal values for Q^2 to reach the optimal trade-off between maximally explained variance and minimal risk of overfitting. After an initial run, the X-variables not reaching the cutoff for Variable Importance for Prediction (VIP) score of 0.8 were deleted from the model[51, 52]. We used the Tomek Sampling method[53] implemented in the JMP Unbalanced Classification add-in to account for the unbalanced nature of the classification problem with a 60/40 HC/FD patient ratio, which indicated the exclusion of 2 HCs from the model.

Similarly, the relationship between the calculated graph measures and selected peripheral metabolites was tested using PLS regression for continuous outcomes. Given the smaller sample size (as not all HC included in the brain imaging analysis have metabolomics data), leave-one-out cross-validation was used in this case rather than k-fold.

Mediation analysis was performed using the PROCESS macro (v5.0[54]) implemented in SAS 9.4 (TS1M7) with 5000 bootstrap iterations.

Functional Connectivity Multivariate Pattern Analysis (fc-MVPA)

Analyses of fMRI data were performed using CONN (RRID:SCR_009550)[32] release 20.b and SPM[33] (RRID:SCR_007037) release 12.7771.

First-level analysis

Functional connectivity multivariate pattern analyses (fc-MVPA) were performed to estimate the first 6 eigenpatterns characterizing the principal axes of heterogeneity in functional connectivity across subjects. From these eigenpatterns, 6 associated eigenpattern-score images were derived for each individual subject characterizing their brain-wide functional connectome state. Eigenpatterns and eigenpattern-scores were computed separately for each individual seed voxel as the left- and right- singular vectors, respectively, from a singular value decomposition (group-level SVD) of the matrix of functional connectivity values between this seed voxel and the rest of the brain (a matrix with one row per target voxel, and one column per subject). Individual functional connectivity values were computed from the matrices of bivariate correlation coefficients between the BOLD timeseries from each pair of voxels, estimated using a singular value decomposition of the z-score normalized BOLD signal (subject-level SVD) with 64 components separately for each subject.

Second-level analyses

Group-level analyses were performed using a General Linear Model (GLM). For each individual voxel a separate GLM was estimated, with first-level connectivity measures at this voxel as dependent variables (one independent sample per subject), and group as independent variable. Voxel-level hypotheses were evaluated using multivariate parametric statistics with random-effects across subjects and sample covariance estimation across multiple measurements. Inferences were performed at the level of individual clusters (groups of contiguous voxels). Cluster-level inferences were based on nonparametric statistics using Threshold Free Cluster Enhancement (TFCE), with 1000 residual-randomization iterations. Results were thresholded using a familywise corrected p-FWE < 0.05 TFCE-score threshold.

Statistical analyses

Linear regression models analyzing between-group differences metabolite, microbiota, dietary or symptom data were preceded by testing for normally distributed residuals. If needed, Box-Cox transformation was applied to continuous dependent and independent variables to meet the requirement of normally distributed residuals. PPI intake nested in the grouping variable was included in models analyzing group effects on symptom scores, dietary estimates and metabolite concentrations. Additionally, metabolite concentration models were adjusted for fiber (SCFA) or protein (AAA and AAA metabolites) intake.

Between-group (FD vs. HC) differences following PCA (*rda* function in R package *vegan*) were analyzed by permutational analysis of variance (PERMANOVA, 10,000 permutations) on the scaled metabolite matrix (all individual metabolites or only microbiota-derived individual metabolites) per sample type (serum or urine) using the *adonis2* function in R package *vegan* with or without adjusting for PPI and protein intake. The explained proportion of variance (R^2) and *P* values were reported.

Associations between symptoms and metabolites of interest (urinary IAA, serum Kyn and plasma propionate) were analyzed by linear regression models while controlling for dietary protein (IAA, Kyn) or fiber (propionate) and PPI intake. Multivariate models were constructed to assess the combined effect of urinary IAA, serum Kyn and plasma propionate on symptoms while controlling for protein and fiber intake. Spearman correlations between the three metabolites of interest were adjusted by Benjamini-Hochberg correction (3 tests, q_{FDR}).

To reduce the complexity of statistical models and to prevent overinterpretation of small differences in stool consistency, Bristol Stool Scale (BSS) score was treated as a categorical variable with three ordinal levels: constipation-like hard stools (BSS 1-2), normal stools (BSS

3-5) and diarrhea-like loose stools (BSS 6-7). The proportion of stool consistency types between groups was compared by Fisher's exact test.

Associations of significantly different metabolites and symptoms between FD and HC with microbiota compositional variation were evaluated using PERMANOVA, with BSS as a fixed covariate in all models. Benjamini-Hochberg correction was applied to adjust for multiple simultaneous comparisons (20 tests) and presented as nominal p-values (*P*) and false discovery rate-adjusted *q*-values (q_{FDR}).

Alpha (within-sample) diversity was analyzed genus-level QMP matrix by calculating the observed richness (number of taxa), Shannon index and inverse Simpson index using the *estimate_richness* function in R package *phyloseq*. Beta (between-sample) diversity was analyzed by principal coordinate analysis (PCoA) based on Bray-Curtis dissimilarity at the genus level using the *ordinate* function in R package *phyloseq*. PERMANOVA with 10,000 permutations using the *adonis2* function in R package *vegan* assessed the main effect of group, PPI intake and BSS on compositional variation.

Differential absolute genera abundance analysis was performed after application of a prevalence cut-off of ≥ 20% across the samples, retaining 68 bacterial genera belonging to 6 phyla. Within this dataset, the percentage of samples with zero-abundant genera ranged from 0% (genus detected in all samples) to 79% (genus detected in 21% of the samples). First, unpaired Mann-Whitney-U tests with Benjamini-Hochberg correction (68 tests, q_{FDR}) were performed to evaluate between-group differences in absolute genera abundances. Effect sizes are reported as rank biserial correlation coefficients (r). Next, negative binomial models (family = nbinom2 using *glmmTMB* function in R package *glmmTMB*) were constructed to account for the specific distribution of QMP data, with inclusion of a zero-inflated term (zi = ~1) for genera that were not zero-inflated. First, 'group' (FD vs. HC) was included as the only independent variable, followed by models where PPI intake nested within 'group' and BSS were included as additional independent variables.

Supplementary results

Limited differences in fecal bacterial taxa abundance between FD and HC

Fecal microbial load did not differ between groups (η_p^2 = 0.008, P = 0.45), although, as expected, it decreased with looser stool consistency (η_p^2 = 0.094, P = 0.030), independent of PPI intake (η_p^2 = 0.005, P = 0.54) (**Supplementary Figure 2B**). Genus-based alpha diversity quantified by the number of observed genera, Shannon index and inverse Simpson index was similar in FD and HC (all P > 0.1) (**Supplementary Figure 2C**), while microbial richness decreased with looser stool consistency (observed genera: η_p^2 = 0.13, P = 0.0068; Shannon index: η_p^2 = 0.077, P = 0.058) (**Supplementary Figure 2D**).

Analysis of differentially abundant bacterial taxa between groups was performed at the genus level, retaining 68 bacterial genera belonging to six phyla after applying a prevalence cutoff of ≥ 20%. Initially, non-parametric tests indicated higher absolute fecal *Butyricicoccus* abundance in FD (r = 0.32, P = 0.02), although no differentially abundant genera persisted after FDR correction (68 tests, all q_{FDR} = 0.99) (**Supplementary Table 7**). To better account for the specific distribution of absolute bacterial taxa abundances, we applied negative binomial models with an additional zero-inflated term for taxa that were not detected in all samples. Univariable analyses for between-group differences pointed toward decreased *Odoribacter* (B ± SE -0.79 ± 0.22, q_{FDR} = 0.023) and *Turicibacter* (-0.90 ± 0.26, q_{FDR} = 0.024) abundance in FD, with a trend for increased *Flavonifractor* (0.71 ± 0.24, q_{FDR} = 0.067) abundance (**Figure 4D**, **Supplementary Table 8**). When also including PPI intake and BSS as additional independent variables, similar trends for decreased *Odoribacter* (-0.68 ± 0.24) and *Turicibacter* (-0.81 ± 0.28), and increased *Flavonifractor* (0.77 ± 0.27; all q_{FDR} = 0.075) persisted, as well as for decreased unclassified *Clostridia* (-1.11 ± 0.37, q_{FDR} = 0.075) (**Figure 4D**, **Supplementary Table 9**). PPI intake at the time of sampling was linked to significantly higher fecal *Streptococcus* (1.38 ± 0.36) abundance, but lower *Bifidobacterium* (-1.43 ± 0.37; both q_{FDR} = 0.0042) abundance (**Figure 4D**, **Supplementary Table 9**). Of note, the absolute *Prevotella* abundance was lower in fecal samples with a hard consistency (BSS 1-2), while loose stools (BSS 6-7) were associated with lower unclassified *Veillonellaceae*, *Collinsella*, *Coprococcus*, *Dorea*, *Oscillibacter* and unclassified *Coriobacteriaceae* abundance (**Figure 4D**, **Supplementary Table 9**).

Fecal microbiota community variation is closely associated with peripheral metabolite profiles

Next, we evaluated if the marked differences between study groups in metabolites and symptoms were associated with the composition of the gut microbiota, especially considering

the microbial origin of various metabolites included in the current analysis. Therefore, we tested for associations between the significantly different metabolites in FD and HC, as well as symptom variables, using PERMANOVA. BSS was included in all models as a covariate given its significant contribution to microbiota compositional variation, which was confirmed in these models (R^2_{BSS} range: 0.045 - 0.058; $P_{PERMANOVA} < 0.031$; $q_{FDR} < 0.031$) (**Supplementary Table 10**). Of all tested symptom variables, only GAD7 tended to be associated with microbiota compositional variation ($R^2 = 0.020$, $q_{FDR} = 0.099$). In contrast, both the aggregated microbial metabolites in serum ($R^2 = 0.048$, $q_{FDR} = 0.047$) and urine ($R^2 = 0.024$, $q_{FDR} = 0.049$), as well as host metabolites in serum ($R^2 = 0.027$, $q_{FDR} = 0.025$) were significantly associated with microbiota composition. Similar significant associations with microbial community variation were found for total plasma SCFA ($R^2 = 0.031$, $q_{FDR} = 0.016$) and individual metabolites (plasma propionate: $R^2 = 0.029$, $q_{FDR} = 0.022$; urinary IAA: $R^2 = 0.023$, $q_{FDR} = 0.049$; urinary PAGln: $R^2 = 0.034$, $q_{FDR} = 0.0090$; serum PAGln: $R^2 = 0.038$, $q_{FDR} = 0.0049$; and serum Kyn: $R^2 = 0.026$, $q_{FDR} = 0.032$) (**Supplementary Table 10**).

Supplementary Figure legends

Supplementary Figure 1: Patients with FD exhibit a distinct serum microbial metabolite profile. Principal component analysis of (**A**) serum microbial AAA metabolites, and (**B**) urinary AAA and AAA metabolites. Permutational analysis of variance (PERMANOVA, 10,000 permutations) quantified explained proportion of variance (R^2) by 'Group'.

Supplementary Figure 2: Stool consistency is associated with fecal microbiota composition. (**A**) Principal coordinate analysis (PCoA, Bray-Curtis) of fecal microbiota samples by stool sample consistency (Bristol Stool Scale, BSS). Permutational analysis of variance (PERMANOVA, 10,000 permutations) quantified explained proportion of variance (R^2) by 'BSS category'. (**B**) Differences in fecal microbial load (flow cytometric microbial cell counts) between groups (left) or BSS category (right). Differences in fecal microbial alpha diversity indices (genus-level) (**C**) between groups or (**D**) by stool sample consistency. Linear regression with main 'Group' effect and 'PPI intake' nested in the grouping variable or main 'BSS category' effect. *P* values represent main 'BSS category' effects (**B**, **D**).

Supplementary Figure 3: Resting-state functional brain connectivity accurately predicts urinary IAA levels. Factor loading plots for (**A**) partial least squares discriminant analysis (PLS-DA) and (**B**) PLS regression analysis using functional connectivity-based graph measures (X-variables). Plots depict Y variables (**A**: FD and HC, **B**: urinary IAA) blue, individual FD (black circles) and HC (black triangles) subject loadings, and 339 or 320 X-variables (green dots) exceeding the Variable Importance for Prediction (VIP) threshold of 0.8 to enter the final PLS-DA and PLS regression models, respectively. (**C**) Linear relationship between observed urinary IAA levels and predicted urinary IAA levels by PLS regression. Pearson correlation coefficient (r) and *P* value as indicated. (**D**) Leave-one-out cross-validation procedure outcomes for urinary IAA, plasma propionate and serum kynurenine (Kyn) suggested a 2-factor solution based on a minimum value for the root mean PRESS statistic for the null model for urinary IAA, while 0 factors were suggested for propionate and Kyn. (**E**) Between-group differences in standardized factors of the PLS regression model explaining 19% and 16% variance in the graph measures, respectively. One-way analysis of variance.

Supplementary references

1. Stanghellini V, Chan FK, Hasler WL, et al. Gastroduodenal Disorders. Gastroenterology 2016;150:1380-92.
2. Rentz AM, Kahrilas P, Stanghellini V, et al. Development and psychometric evaluation of the patient assessment of upper gastrointestinal symptom severity index (PAGI-SYM) in patients with upper gastrointestinal disorders. Qual Life Res 2004;13:1737-49.
3. Carbone F, Vandenberghe A, Holvoet L, et al. Validation of the Leuven Postprandial Distress Scale, a questionnaire for symptom assessment in the functional dyspepsia/postprandial distress syndrome. Aliment Pharmacol Ther 2016;44:989-1001.
4. Spitzer RL, Kroenke K, Williams JB, et al. A brief measure for assessing generalized anxiety disorder: the GAD-7. Arch Intern Med 2006;166:1092-7.
5. Kroenke K, Spitzer RL, Williams JB. The PHQ-9: validity of a brief depression severity measure. J Gen Intern Med 2001;16:606-13.
6. Cohen S, Kamarck T, Mermelstein R. A global measure of perceived stress. J Health Soc Behav 1983;24:385-96.
7. Labus JS, Bolus R, Chang L, et al. The Visceral Sensitivity Index: development and validation of a gastrointestinal symptom-specific anxiety scale. Aliment Pharmacol Ther 2004;20:89-97.
8. Blevins CA, Weathers FW, Davis MT, et al. The Posttraumatic Stress Disorder Checklist for DSM-5 (PCL-5): Development and Initial Psychometric Evaluation. J Trauma Stress 2015;28:489-98.
9. Bernstein DP, Fink L, Handelsman L, et al. Initial reliability and validity of a new retrospective measure of child abuse and neglect. Am J Psychiatry 1994;151:1132-6.
10. Watson D, Clark LA, Tellegen A. Development and validation of brief measures of positive and negative affect: the PANAS scales. J Pers Soc Psychol 1988;54:1063-70.
11. Spiller RC, Humes DJ, Campbell E, et al. The Patient Health Questionnaire 12 Somatic Symptom scale as a predictor of symptom severity and consulting behaviour in patients with irritable bowel syndrome and symptomatic diverticular disease. Aliment Pharmacol Ther 2010;32:811-20.
12. Vandeputte D, Kathagen G, D'Hoe K, et al. Quantitative microbiome profiling links gut community variation to microbial load. Nature 2017;551:507-511.
13. Tito RY, Verbandt S, Aguirre Vazquez M, et al. Microbiome confounders and quantitative profiling challenge predicted microbial targets in colorectal cancer development. Nat Med 2024;30:1339-1348.

14. Hildebrand F, Tadeo R, Voigt AY, et al. LotuS: an efficient and user-friendly OTU processing pipeline. Microbiome 2014;2:30.
15. Callahan BJ, McMurdie PJ, Rosen MJ, et al. DADA2: High-resolution sample inference from Illumina amplicon data. Nat Methods 2016;13:581-3.
16. Esteban O, Markiewicz CJ, Blair RW, et al. fMRIPrep: a robust preprocessing pipeline for functional MRI. Nat Methods 2019;16:111-116.
17. Gorgolewski K, Burns CD, Madison C, et al. Nipype: a flexible, lightweight and extensible neuroimaging data processing framework in python. Front Neuroinform 2011;5:13.
18. Tustison NJ, Avants BB, Cook PA, et al. N4ITK: improved N3 bias correction. IEEE Trans Med Imaging 2010;29:1310-20.
19. Avants B, Tustison N, Song G. Advanced normalization tools (ANTS). Insight J 2008;1–35.
20. Zhang Y, Brady M, Smith S. Segmentation of brain MR images through a hidden Markov random field model and the expectation-maximization algorithm. IEEE Trans Med Imaging 2001;20:45-57.
21. Fonov VS, Evans AC, McKinstry RC, et al. Unbiased nonlinear average age-appropriate brain templates from birth to adulthood. NeuroImage 2009;47:S102.
22. Jenkinson M, Smith S. A global optimisation method for robust affine registration of brain images. Med Image Anal 2001;5:143-56.
23. Greve DN, Fischl B. Accurate and robust brain image alignment using boundary-based registration. Neuroimage 2009;48:63-72.
24. Jenkinson M, Bannister P, Brady M, et al. Improved optimization for the robust and accurate linear registration and motion correction of brain images. Neuroimage 2002;17:825-41.
25. Cox RW, Hyde JS. Software tools for analysis and visualization of fMRI data. NMR Biomed 1997;10:171-8.
26. Power JD, Mitra A, Laumann TO, et al. Methods to detect, characterize, and remove motion artifact in resting state fMRI. Neuroimage 2014;84:320-41.
27. Behzadi Y, Restom K, Liau J, et al. A component based noise correction method (CompCor) for BOLD and perfusion based fMRI. Neuroimage 2007;37:90-101.
28. Satterthwaite TD, Elliott MA, Gerraty RT, et al. An improved framework for confound regression and filtering for control of motion artifact in the preprocessing of resting-state functional connectivity data. Neuroimage 2013;64:240-56.
29. Lanczos C. Evaluation of Noisy Data. Journal of the Society for Industrial and Applied Mathematics Series B Numerical Analysis 1964;1:76-85.

30. Abraham A, Pedregosa F, Eickenberg M, et al. Machine learning for neuroimaging with scikit-learn. Front Neuroinform 2014;8:14.
31. developers Tf. Processing pipeline details. Volume 2025, 2016.
32. Whitfield-Gabrieli S, Nieto-Castanon A. Conn: a functional connectivity toolbox for correlated and anticorrelated brain networks. Brain Connect 2012;2:125-41.
33. Friston KJ, Holmes AP, Worsley KJ, et al. Statistical parametric maps in functional imaging: A general linear approach. Human Brain Mapping 1994;2:189-210.
34. Oishi K, Faria A, Jiang H, et al. Atlas-based whole brain white matter analysis using large deformation diffeomorphic metric mapping: application to normal elderly and Alzheimer's disease participants. Neuroimage 2009;46:486-99.
35. Mayer EA, Labus J, Aziz Q, et al. Role of brain imaging in disorders of brain-gut interaction: a Rome Working Team Report. Gut 2019;68:1701-1715.
36. Lee IS, Wang H, Chae Y, et al. Functional neuroimaging studies in functional dyspepsia patients: a systematic review. Neurogastroenterol Motil 2016;28:793-805.
37. Mao Y, Zhang P, Sun R, et al. Altered resting-state brain activity in functional dyspepsia patients: a coordinate-based meta-analysis. Front Neurosci 2023;17:1174287.
38. Sun R, Zhou J, Qu Y, et al. Resting-state functional brain alterations in functional dyspepsia: Protocol for a systematic review and voxel-based meta-analysis. Medicine (Baltimore) 2020;99:e23292.
39. Zeng F, Qin W, Yang Y, et al. Regional brain structural abnormality in meal-related functional dyspepsia patients: a voxel-based morphometry study. PLoS One 2013;8:e68383.
40. Nan J, Liu J, Zhang D, et al. Altered intrinsic regional activity and corresponding brain pathways reflect the symptom severity of functional dyspepsia. Neurogastroenterol Motil 2014;26:660-9.
41. Nan J, Zhang L, Zhu F, et al. Topological Alterations of the Intrinsic Brain Network in Patients with Functional Dyspepsia. J Neurogastroenterol Motil 2016;22:118-28.
42. Liu P, Wang G, Zeng F, et al. Abnormal brain structure implicated in patients with functional dyspepsia. Brain Imaging Behav 2018;12:459-466.
43. Nan J, Liu J, Li G, et al. Whole-brain functional connectivity identification of functional dyspepsia. PLoS One 2013;8:e65870.
44. Zeng F, Qin W, Liang F, et al. Abnormal resting brain activity in patients with functional dyspepsia is related to symptom severity. Gastroenterology 2011;141:499-506.
45. Kruschwitz JD, List D, Waller L, et al. GraphVar: a user-friendly toolbox for comprehensive graph analyses of functional brain connectivity. J Neurosci Methods 2015;245:107-15.

46. Waller L, Brovkin A, Dorfschmidt L, et al. GraphVar 2.0: A user-friendly toolbox for machine learning on functional connectivity measures. J Neurosci Methods 2018;308:21-33.
47. Wee CY, Yap PT, Zhang D, et al. Group-constrained sparse fMRI connectivity modeling for mild cognitive impairment identification. Brain Struct Funct 2014;219:641-56.
48. Zhou Z, Chen X, Zhang Y, et al. A toolbox for brain network construction and classification (BrainNetClass). Hum Brain Mapp 2020;41:2808-2826.
49. Storey JD. A direct approach to false discovery rates. Journal of the Royal Statistical Society: Series B (Statistical Methodology) 2002;64:479-498.
50. Storey JD, Taylor JE, Siegmund D. Strong Control, Conservative Point Estimation and Simultaneous Conservative Consistency of False Discovery Rates: A Unified Approach. Journal of the Royal Statistical Society Series B: Statistical Methodology 2003;66:187-205.
51. Eriksson L, Byrne T, Johansson E, et al. Multi-and megavariate data analysis basic principles and applications: Umetrics Academy, 2013.
52. Wold S, Eriksson L. Chemometric methods in molecular designmethods and principles in medicinal chemistry. PLS for multivariate linear modeling 1995:195-218.
53. He H, Garcia EA. Learning from imbalanced data. IEEE Transactions on knowledge and data engineering 2009;21:1263-1284.
54. Hayes AF. Introduction to mediation, moderation, and conditional process analysis. New York: Guilford Press, 2017.

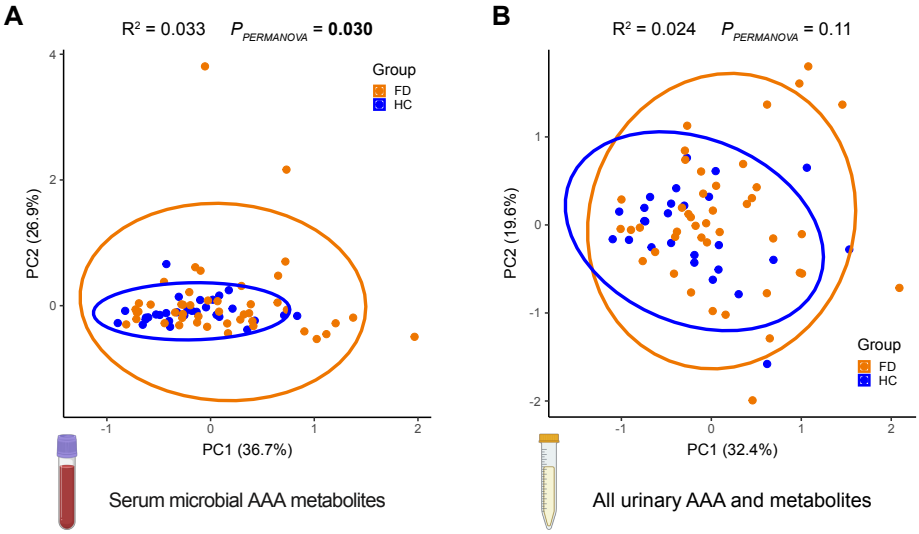
A
R² = 0.033 P PERMANOVA = 0.030
Group
FD
HC
PC2 (26.9%)
PC1 (36.7%)
Serum microbial AAA metabolites
B
R² = 0.024 P PERMANOVA = 0.11
Group
FD
HC
PC2 (19.6%)
PC1 (32.4%)
All urinary AAA and metabolites

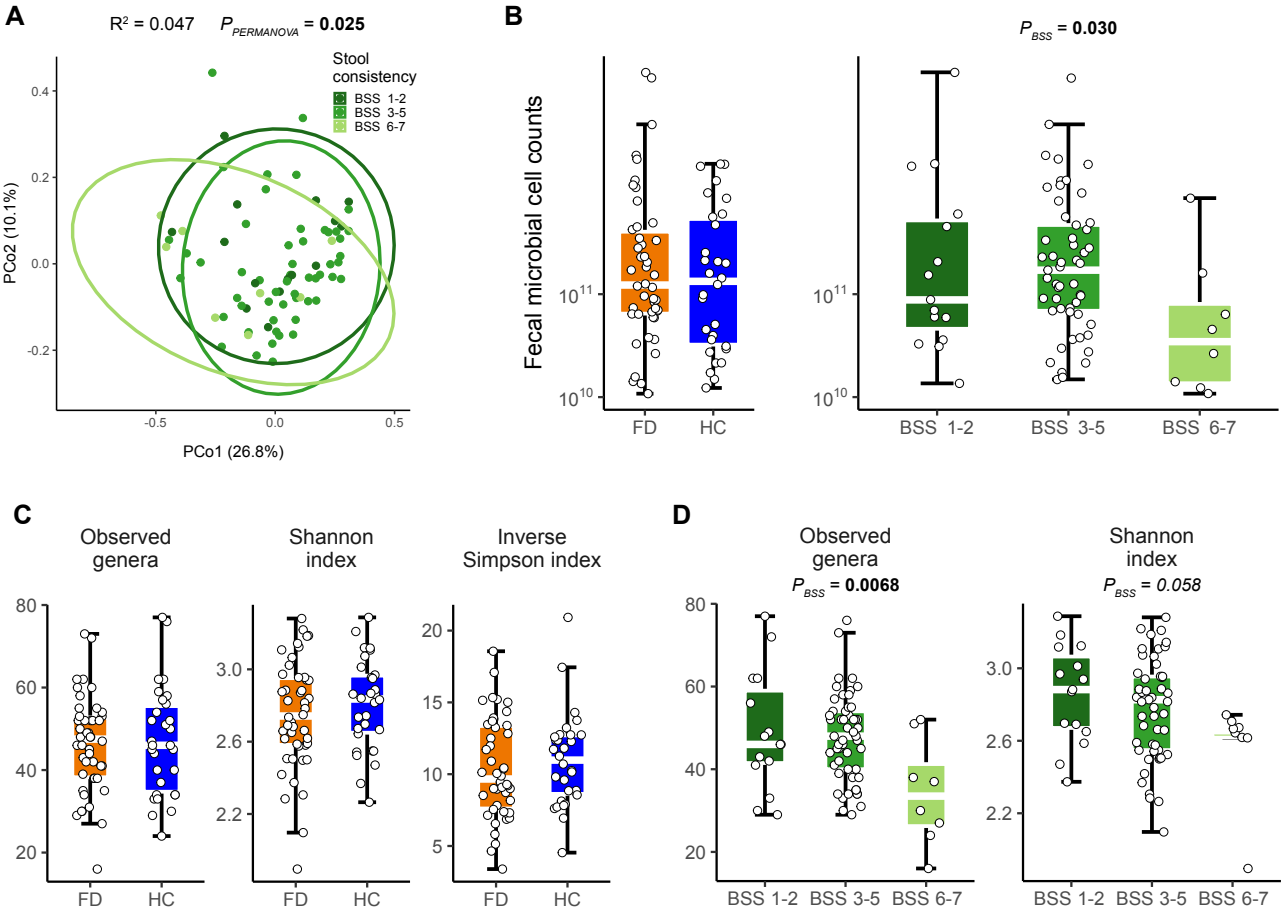
A
R² = 0.047
P_PERMANOVA = 0.025
Stool consistency
BSS 1-2
BSS 3-5
BSS 6-7
PCo2 (10.1%)
PCo1 (26.8%)
B
P_BSS = 0.030
Fecal microbial cell counts
FD
HC
BSS 1-2
BSS 3-5
BSS 6-7
C
Observed genera
Shannon index
Inverse Simpson index
D
Observed genera
P_BSS = 0.0068
Shannon index
P_BSS = 0.058

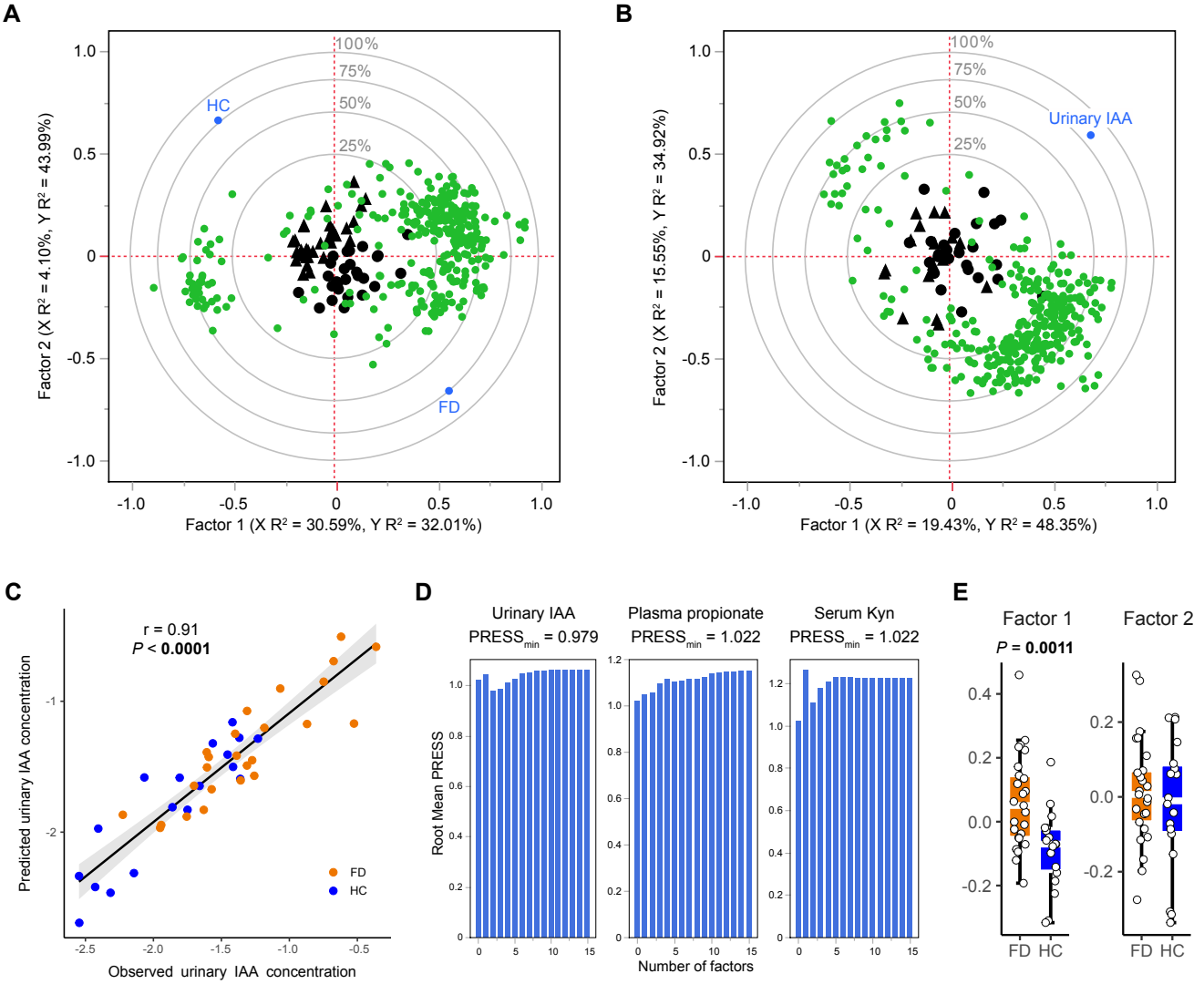
A
100%
75%
50%
25%
HC
FD
Factor 2 (X R² = 4.10%, Y R² = 43.99%)
Factor 1 (X R² = 30.59%, Y R² = 32.01%)
B
Urinary IAA
Factor 2 (X R² = 15.55%, Y R² = 34.92%)
Factor 1 (X R² = 19.43%, Y R² = 48.35%)
C
r = 0.91
P < 0.0001
FD
HC
Predicted urinary IAA concentration
Observed urinary IAA concentration
D
Urinary IAA
PRESSmin = 0.979
Plasma propionate
PRESSmin = 1.022
Serum Kyn
PRESSmin = 1.022
Root Mean PRESS
Number of factors
E
Factor 1
P = 0.0011
Factor 2
FD
HC